RAMAN AMPLIFICATION AND SUPERCONTINUUM GENERATION IN PHOTONIC CRYSTAL FIBER

A Dissertation Submitted towards the Partial Fulfillment of

the Award of Degree of

MASTER OF TECHNOLOGY

in

MICROWAVE AND OPTICAL COMMUNICATION ENGINEERING

by

VINIT KUMAR
(2K09/MOC/17)

DEPARTMENT OF ELECTRONICS AND COMMUNICATION
&
DEPARTMENT OF APPLIED PHYSICS
DELHI TECHNOLOGY UNIVERSITY (FORMERLY DCE)
JUNE 2011

RAMAN AMPLIFICATION AND SUPERCONTINUUM GENERATION IN PHOTONIC CRYSTAL FIBER

A Dissertation Submitted towards the Partial Fulfillment of

the Award of Degree of

MASTER OF TECHNOLOGY

in

MICROWAVE AND OPTICAL COMMUNICATION ENGINEERING

by

VINIT KUMAR
(2K09/MOC/17)

Dr. R. K. Sinha
Professor
DEPARTMENT OF APPLIED PHYSICS
DELHI TECHNOLOGY UNIVERSITY (FORMERLY DCE)
JUNE 2011

Certificate

This is to certify that the dissertation titled '*Raman amplification and Supercontinuum generation in photonic crystal fiber*' being submitted by **VINIT KUMAR** to the Delhi technological university (formerly DCE) is a record of bonafide research work carried out by him. He has worked under our guidance and fulfils the requirements of the regulations laid down for the purpose of award of the degree. The contents of this thesis have not been submitted to any other University or Institute for the award of any degree or diploma.

Prof. R.K. Sinha
HOD
Department of Applied Physics

DTU

Prof. Rajiv Kapoor
HOD
Department of Electonics & Communication Engineering
DTU

Acknowledgement

The completion of this project has come through the overwhelming help that came from many people. I wish to express my sincere gratitude to all the people who offered their kind help and guidance throughout my project period.

I am deeply indebted to my supervisor **Prof R.K. Sinha** for all the advice, support , vast experience and guidance , he has provide me. It has been privileged to have work with him. As my supervisor , he has constantly forced me to remain focused on achieving my goal. He has taken their busy time out to go through my thesis and gave his valuable suggestions.

I would also like to place on record , my thanks to the Electronics and Communication and Physics Department for making available the facilities required for carrying out this study. A special mention goes to the Lab Staff in this regard.

In my daily work I have been blessed with a friendly and cheerful group of fellow students and I wish to thank them for the support and assistance provided by them during the course of this project.

Lastly, I thanks to my family whose constant support has been a pillar of strength for me throughout this study.

Vinit Kumar
M.Tech (Microwave and Optical Communication)
Delhi Technological University (Formerly DCE)
Bawana Road, Delhi –110042
India.

List of symbols

α	Fiber loss
λp	Pump wavelength
λ_{FWM}	Wavelength generated through FWM
λ_{ZD}	Zero-dispersion wavelength
β	Propagation constant
γ	Nonlinear coefficient
ε_0	Vacuum permittivity
λ	Wavelength
μ_0	Vacuum permeability
L	Fiber length
L_D	Dispersion length
L_{NL}	Nonlinear fiber length
N	Soliton order
P	Polarization
Pp	Peak power
β_2	Second-order dispersion
β_k	k^{th} order dispersion
SNR	Signal to noise ratio
S_{out}	Output signal
N_{in}	Input noise
S_{in}	Input signal
B_{opt}	Bandwidth of optical filter
ASE	Amplified spontaneous noise
NF	Noise figure
N_{out}	Output noise
G_A	Raman gain

P_s	Signal power
T_0	Temporal width
w_p	Frequency of the pump
w_{as}	Frequency of the anti-Stokes
w_{st}	Frequency of the Stokes Photons
w_{off}	Offset frequency
h_R	Raman response function
R (t)	Nonlinear response function
f_r	Phase of the resonant wave
f_s	Phase of the soliton wave
PCF	Photonic crystal fiber
SS	Self steepening
XPM	Cross phase modulation
FWHM	Full width half-maxima
FWM	Four wave mixing
SRS	Stimulated Raman scattering
SPM	Self phase modulation
SC	Supercontinuum
v_s	Signal photon
v_p	Pump photon
$\omega_{s/p}$	Angular frequency of signal and power
$\alpha_{s/p}$	Attenuation coefficient of signal and power
L_{eff}	Effective length
g_R	Raman gain co-efficient

List of figures

Abstract

Photonic Crystal Fibers are single material optical fibers with an array of periodic array of air holes running down its entire length. By leaving a single lattice site without an air hole, a localized region, which has a higher refractive index than the rest of the structure, will be formed. These fibers are being in active research because of its unusual & attractive optical properties like single mode operation in wide wavelength range, large mode area, excitation of non-linear effects at small mode area, and manageable dispersion properties etc. which are not achieved in standard silica glass fiber. Non-silica glasses such as telluride, fluoride and chalcogenide glasses have been used for formation of PCF because of its excellent optical transparency in the longer wavelength infrared (IR) region. In this project, we present the raman gain characteristic and Supercontinuum generation (SCG) in non-linear photonic crystal fibers (PCFs) by using the RSOFT(optisim) software.

To design the nonlinear PCF here we considered the new material i.e. telluride glass. The nonlinear refraction coefficients n_2 of telluride glass is 42 times higher than that of silica. The variation of effective index of guided mode and dispersion with wavelength in hexagonal lattice telluride glass PCF is calculated by using finite element method (FEM).

The raman gain characteristics of Telluride PCF is calculated by using Rsoft-optisim software. We also compare the gain characteristics of telluride glass PCF with conventional silica PCF and find out that the Raman gain in Telluride PCFs can be highly improved than silica PCF. For SCG I reproduce the result of Dudley et al. (2006) with the help of RSOFT Optisim software and also show the effect of varying the power and pulse width on the bandwidth of the spectra.

Table of Contents

CHAPTER 1

PHOTONIC CRYSTAL FIBER

1.1 INTRODUCTION:-

Communication may be broadly defined as the transfer of information from one point to another. When the information is to be conveyed over any distance a communication system is requires. Within a communication system the information transfer is frequently achieved by superimposing or modulating the information on to an electromagnetic wave which acts as a carrier for the information signal. An optical fiber communication system is similar basic concept to any type of communication system.

An optical fiber is a cylindrical dielectric waveguide that transmits light along its axis, by the process of total internal reflection. The fiber consists of a *core* surrounded by a cladding layer, both of which are made of dielectric materials. To confine the optical signal in the core, the refractive index of the core must be greater than that of the cladding. Light pulses move easily down the fiber-optic line because of a principle known as total internal reflection.

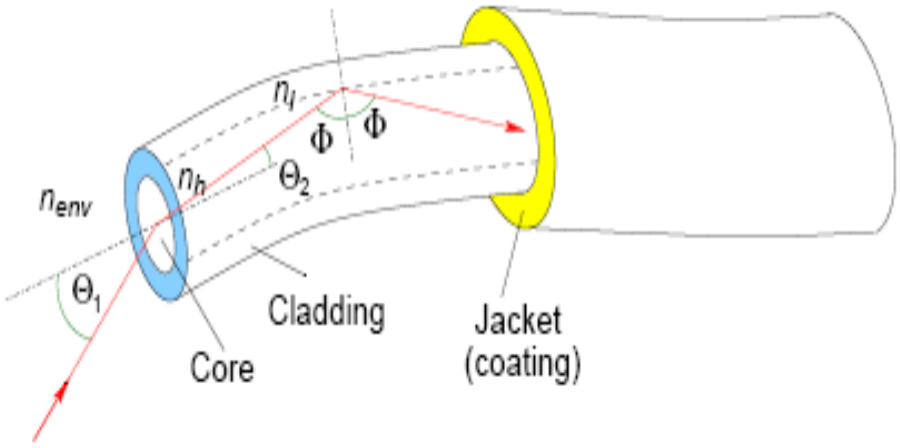

Fig:1. Silica fiber [4]

Fibers are classified according to the number of modes that they can propagate.

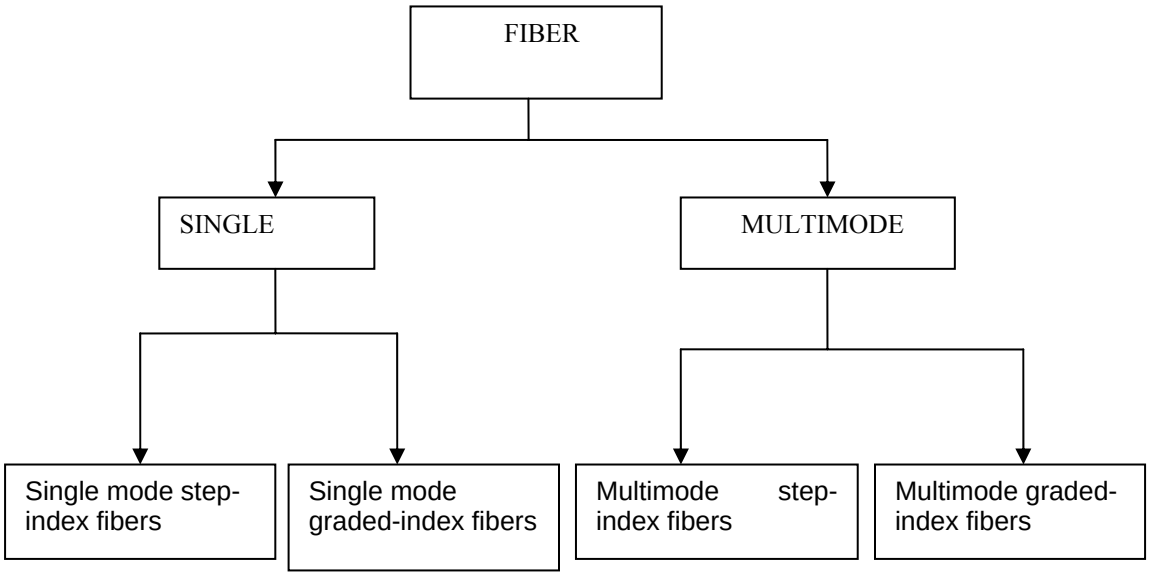

1.1.1Single mode fiber :-

Single mode fibers can propagate only the fundamental mode means only one mode, because the core size approaches the operational wavelength .

(a) The core size (diameter) of single mode fiber is typically around 8 to 10 mi cro meters. A fiber core of this size allows only the fundamental or lowest order mode to propagate around a 1300 nanometer (nm) wavelength.

(b) The value of the normalized frequency parameter (V) relates core size with mode propagation. In single mode fibers, V is less than or equal to 2.405.

(c) Single mode fibers have a lower signal loss and a higher information capacity (bandwidth) than multimode fibers. Single mode fibers are capable of transfer ring higher amounts of data due to low fiber dispersion

1.1.2Multimode fiber:-

Multimode fibers can propagate hundreds of modes. As their name implies, multimode fibers propagate more than one mode. Multimode fibers can propagate over 100 modes.

(a) The core size (diameter) of multimode mode fiber is typically around 50 to 100 μm.

(b) The value of the normalized frequency parameter (V) relates core size with mode propagation. In single mode fibers, V is greater than 2.405.

(c) The number of modes propagated depends on the numerical aperture (NA). As the NA increase, the number of modes increases. Typical values of NA is 0.20 to 0.29, respectively.

Classical optical fibers perform very well in telecom and non-telecom applications, but there is a series of fundamental limits related to their structures. The fibers have rigid design rules to fulfill: limited core diameter in the single-mode regime, modal cut-off wavelength, limited material choice (thermal properties of core glass and cladding glass must be the same). Now a days, research is focus on the use of single material for the formation of optical fiber known as Photonic crystal fiber (PCF). The design of PCFs is very flexible. In PCF we are easily able to manipulate several parameters like: lattice pitch (hole-to-hole spacing), air hole shape and diameter, refractive index of the glass, and type of lattice. Freedom of design allows one to obtain *endlessly single mode fibers*, which are single mode in all optical range and a cut-off wavelength does not exist. Combining properties of optical fibers and photonic crystals they possess a series of unique properties impossible to achieve in classical fibers.

1.1.3 PHOTONIC CRYSTAL FIBER:-

With growing demand of high speed, large speed, large bandwidth, miniaturization of circuits, scientists throughout the world switching over to light because light has several advantages compared to electrons. Inspite of numerous advantages of photons, all optical circuits have yet to become commercially available on a large scale. A new class of optical materials, known as Photonic Crystals (PCs) or photonic bandgap materials, holds the key for the development of novel all optical integrated circuits of small dimensions. PCs are artificial structures employing a periodic structure designed to influence the behavior of photons in the same way as a semiconductor crystal affects the properties of electrons.

Photonic Crystal Fibers are single material optical fibers with an array of periodic array of air holes running down its entire length. The idea of a photonic crystal fiber was presented for the first time by Yeh et al. in 1978. They proposed to clad a fiber core with Bragg grating, which is similar to 1D photonic crystal. A photonic crystal fiber made of 2D photonic crystal with an air core was invented by P. Russell in 1992 and the first PCF was reported at the Optical Fiber Conference (OFC) in 1996 .

By leaving a single lattice site without an air hole, a localized region, which has a higher refractive index than the rest of the structure, will be formed. This localized region acts as a waveguide core in which light can be trapped along the axis of the fiber. PCF uses the photonic crystal cladding as an effective index medium to form wave guiding cladding. The regularity of photonic crystal cladding allows one to treat it as an effective medium which facilitates the analysis of the properties of the medium and hence the wave guiding characteristics. The unusual properties of PCFs arise from the strong wavelength dependence of the effective cladding index. There are two guiding mechanisms in PCF: index

guiding mechanism (similar to the one in classical optical fibers) and the photonic bandgap mechanism. By manipulating the structure it is possible to design desired dispersion properties of the fiber. PCFs having zero, low, or anomalous dispersion at visible wavelengths can be designed and fabricated. The dispersion can also be fattened over a very large range. Combining anomalous dispersion with small mode field areas results in outstanding nonlinear fibers. On the other hand large, solid or air core single mode fibers can be achieved.

1.1.4 Overview of photonic crystal fibers development:-

1978 Idea of the Bragg fiber

1992 Idea of the photonic crystal fiber with air core

1996 Fabrication of a single-mode fiber with photonic coating

1997 Endlessly singe mode PCF

1999 PCF with photonic bandgap and air core

2000 Highly birefringent PCF

2000 Supercontinuum generation with PCF

2001 Fabrication of a Bragg fiber

2001 PCF laser with double cladding

2002 PCF with ultra-fattened dispersion

2003 Bragg fiber with silica and air core

1.2. Theory:-

In standard optical fibers, the parameter which is most often discussed is the propagation constant β along the direction of the fiber axis. When there is no change in the structure along this direction, light launched with a given β will maintain this value throughout the entire length. In order to form a mode which is guided in the core of the structure, the light must have a $\beta \leq n_{cl}\, k_o$ where n_{cl} is the index of the cladding and k_o is the propagation constant in free space, $k = 2\pi\, \lambda_o$. From this value of β , it is also common to define an effective index of the mode, where $n_{eff} = \beta / k_o$. Depending on the structure of the waveguide, there will be a certain range of effective indices, or propagation constants, which are allowed to propagate. In a normal fiber, where the core index is greater than the cladding, guided modes can propagate in a range of effective indices between the index of the core and the cladding. This is also the case for the structure on the left in (figure), where the index of the cladding can be thought of as being reduced by the presence of the air-holes . For the hollow core fiber, there are, depending on the makeup of the structure, bands of allowed and disallowed effective indices or propagation constants which can propagate.

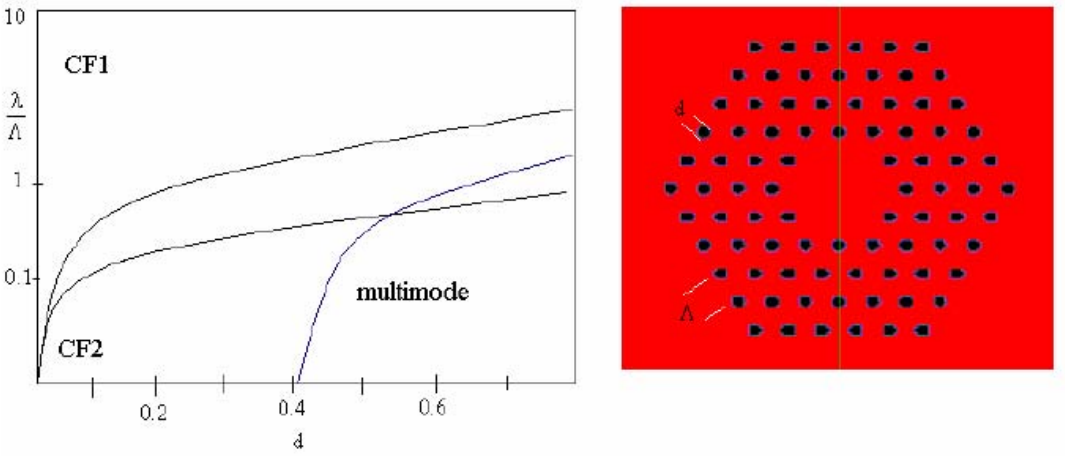

Figure2 . Diagram showing behavior of glass core/air hole fiber. [5]

In the glass core/ air hole structure, the primary difference between this, and the ordinary fiber is the distinction between a guided and an unguided mode . In traditional fibers guided modes have real propagation constants and are lossless, while non-guided modes have a complex β where the imaginary part is related to the loss.

In the micro-structured fibers, all modes experience some tunneling effects due to the periodicity of the holes and thus have complex β and effective indices. From experimental data gathered by reference the diagram below was developed. In the above figure there are four primary sections of interest with regards to the behaviour of light in the above structure. The blue line of course represents where the fiber becomes multi-mode. In the region CF1, it has been shown that the fundamental guided mode fills the entire cross section of the fiber and behaves according to traditional fiber optic theory. In the region CF2, the mode is more strongly confined to the core and also behaves according to classical theories . It is the portion of the above figure which falls between the two black lines which becomes very different from traditional fibers and starts to display a strong sensitivity to parameters such as d the hole width, Λ the pitch, and also the number of rings of the structure rN. The point at which the fiber becomes multimode is of great importance in designing a structure for the guidance of light. In standard optical fibers, such as the step-index fiber, a parameter known as the V-number is often used to characterize this point. This well known equation is

$$V(\lambda) = \frac{2\pi r}{\lambda}\sqrt{n_{core}{}^2 - n_{cladding}{}^2}$$

where r is the core radius of the fiber. In photonic crystal fibers (PCF) the radius of the core is not well defined. However, an expression for the V-number for these micro-structured fibers has recently been derived by reference as

$$V_{PCF}(\lambda) = \frac{2\pi\Lambda}{\lambda}\sqrt{n_c{}^2 - n_{cl}{}^2}$$

where n_c is the effective core index for the fundamental mode and n_{cl} is similarly the effective index of the fundamental “space-filling mode”.

1.3.Types of PCF:-

1.3.1 Solid core PCF:- These fibers, also known as index-guiding PCFs, guide light through a form of total internal reflection (TIR), called modified TIR. In index- guiding PCFs, light is trapped in a high index core by a mechanism similar to the total internal reflection in standard fibers. The cladding region consists of a hexagonal array of airholes, with a missing air hole defining the core. An attractive property of the silica PCFs is that effective index contrasts much higher than in standard fibers may be obtained by making the airholes large, and/or by making the fiber dimensions small so that the light is forced into the airholes . In this way ,strong mode confinement can be obtained, which in turns leads to enhanced **nonlinear effects** due to high field intensity in the core.

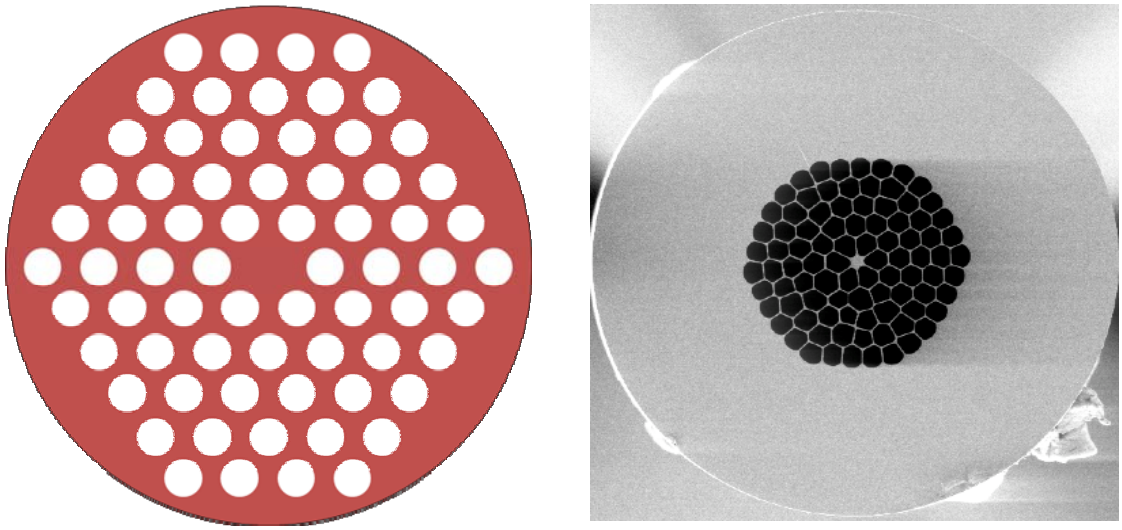

Fig3:- SOLID CORE FIBER [12]

Guiding Mechanism OF Solid core PCF:- In order to form a guided mode in an optical fiber, it is necessary to introduce light into the core with a value of β, that is the component of the propagation constant along the fiber axis, which cannot propagate in the cladding. The highest value that can exist in an infinite homogeneous medium with refractive index n is $\beta = nk_0$, being k_0 the free-space propagation constant. All the smaller values of β are allowed.

If the defect of the structure is realized by removing the central capillary, then guiding of an electromagnetic wave in a photonic crystal fiber can be regarded as a modified total internal refection mechanism. The modification is due to the network of air capillaries that leak higher modes so that only one fundamental mode is carried. This is the mode with the smallest diameter, close to the size of the defect, i.e., to the lattice constant of the periodic structure. A fiber is single-mode if $d/\Lambda < 0.4$, where d is the diameter of the air channel and Λ is the crystal lattice constant. The guiding of light in a photonic crystal fiber was first demonstrated in 1996 in a solid-core fiber (*solid core guidance*) .In a lattice of air capillaries, the central one was replaced by a rod.

As shown in Figure , another design is to use solid-core photonic crystal fiber. This structure refracts light at steep angles of incidence on the core-cladding boundary. When the angle is shallow enough, light is trapped in the core and guided along the fiber.

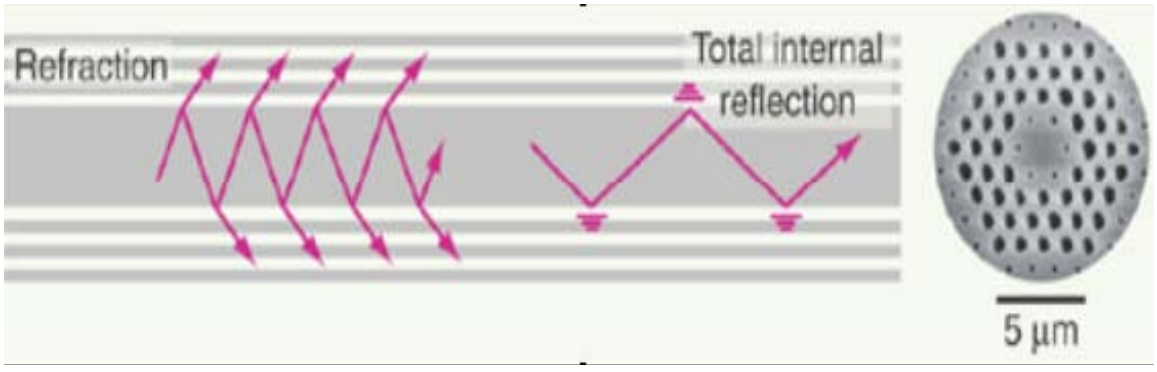

Fig4:- Guiding mechanism in solid core fiber [12]

1.3.2 Hollow core PCF:- Hollow-core optical fibers are able to guide light in an air core by using the photonic bandgap guidance mechanism. The air core is surrounded by a microstructure that typically consists of a pattern of air holes extending longitudinally along the fiber. The microstructure has photonic bandgaps, and light of wavelengths corresponding to these is strongly reflected by the microstructure and guided in the core of the fiber.

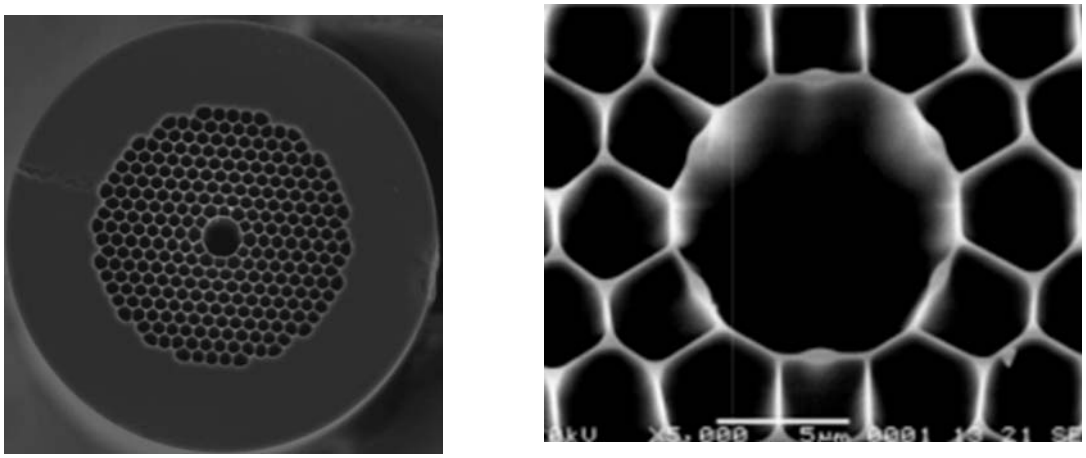

Fig5:- Hollow core fiber [12]

Guiding Mechanism OF Hollow core PCF:-If the central defect is realized by inserting a central air capillary, which has a diameter different than other capillaries (usually bigger), then we can obtain a *photonic bandgap* (PBG). Light guidance is then an analogue of a mechanism known in solid state physics as the electron conduction mechanism in materials with an energy-band structure. In 1997 the guiding of light in an air defect was demonstrated (*hollow core PGB guidance*). A few central capillaries were removed from a hexagonal lattice leaving a large hole filled with air. Periodically distributed air cores can form an artificial 2D photonic crystal structure with lattice constant similar to the wavelength of light. In the 2D crystal structures photonic band gaps exist that prevent propagation of light with a certain range of frequencies. If periodicity of the structure is broken with a defect (lack of air cores or large air core) a special region with optical properties different from the photonic crystal is created. The defect region can

support modes with frequencies falling inside photonic bandgap, which prevent them from penetration of photonic crystal. The modes are strongly confined to the defects and guided along them through the fiber. Since photonic bandgap is responsible for confinement of the light in the core, it is not required that the defect region has a higher refractive index than the surrounding.

Figure shows a hollow-core photonic crystal fiber with an appropriately formed cladding . This structure can guide light at angles of incidence where a photonic band gap operates, but otherwise refracts like a hollow-core capillary.

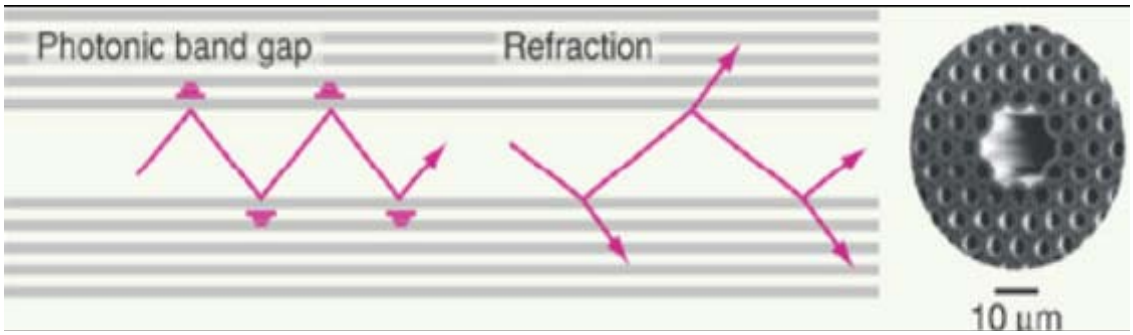

Fig6:- Guiding mechanism in solid core fiber [12]

1.4. Modeling methods

Commonly used methods for modeling of optical fibers cannot be applied successfully in PCF modeling. These fibers have a high refractive index contrast and a subwavelength periodical structure. Therefore, the methods used in modeling photonic crystals and electromagnetic fields are adapted to this purpose.

4.1 OPTI FDTD:-

The finite difference time domain (FDTD) method is widely used for calculation of the evaluation of an electromagnetic field in depressive media . The wave propagation through the PCF structure is found by direct integration in the time domain of Maxwell's equations in a discrete form. Space and time is discrete in a regular grid. Evaluation of the electrical and magnetic field is calculated on a Yee

cell. In addition the boundary conditions are added (absorbing or periodic ones). Most often uniaxial perfect matching layer (UPML) boundary conditions are used for PCF modeling. The method allows obtaining transmission and refection coefficients, energy flow of propagation fields (Pointing vector). It allows the observation of a steady state field distribution as well as the temporary field distribution.

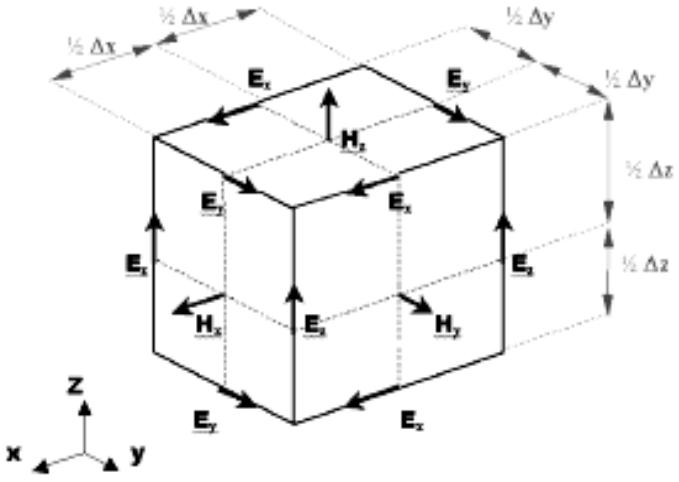

Fig7:-The Yee cell describes all components of electrical and magnetic field in a cube. Every component of the electromagnetic field is defined only in one place in the unit Yee cell.

The FDTD method is universal, robust, and methodologically simple. The main drawback of this method is very high time and memory complexity of the algorithm. Since PCF are 3D structures with 2D refractive index distribution only short pieces of the fiber can be simulated with these methods. It can be successfully applied to model tapers, couplers, and double core coupling in the PCFs. Large volume simulations can be performed with computer clusters because the FDTD method can be relatively easily implemented as a parallel algorithm.

3D FDTD Equations

In 3D simulations, the simulation domain is a cubic box, the space steps are, and in x, y, and z directions respectively. Each field components is presented by a 3D array ---$E_X(i,j,k)$, $E_y(i,j,k)$, $E_Z(i,j,k)$, $H_x(i,j,k)$, $H_y(i,j,k)$, $H_Z(i,j,k)$**.** The field components position in Yee's Cell are shown in fig .

$$H^{n+\frac{1}{2}}_{x,i,j-\frac{1}{2},k-\frac{1}{2}} = H^{n-\frac{1}{2}}_{x,i,j-\frac{1}{2},k-\frac{1}{2}} + \frac{\Delta t}{\mu_o \Delta z}(E^n_{y,i,j-\frac{1}{2},k} - E^n_{y,i,j-\frac{1}{2},k-1}) - \frac{\Delta t}{\mu_o \Delta y}(E^n_{z,i,j,k-\frac{1}{2}} - E^n_{z,i,j-1,k-\frac{1}{2}})$$

$$H^{n+\frac{1}{2}}_{y,i-\frac{1}{2},j,k-\frac{1}{2}} = H^{n-\frac{1}{2}}_{y,i-\frac{1}{2},j,k-\frac{1}{2}} + \frac{\Delta t}{\mu_o \Delta x}(E^n_{z,i,j,k-\frac{1}{2}} - E^n_{z,i-1,j,k-\frac{1}{2}}) - \frac{\Delta t}{\mu_o \Delta z}(E^n_{x,i-\frac{1}{2},j,k} - E^n_{x,i-\frac{1}{2},j,k-1})$$

$$H^{n+\frac{1}{2}}_{z,i-\frac{1}{2},j-\frac{1}{2},k} = H^{n-\frac{1}{2}}_{y,i-\frac{1}{2},j-\frac{1}{2},k} + \frac{\Delta t}{\mu_o \Delta y}(E^n_{x,i-\frac{1}{2},j,k} - E^n_{x,i-\frac{1}{2},j-1,k}) - \frac{\Delta t}{\mu_o \Delta x}(E^n_{y,i,j-\frac{1}{2},k} - E^n_{y,i-1,j-\frac{1}{2},k})$$

1.1

$$E^{n+1}_{x,i-\frac{1}{2},j,k} = \frac{2\varepsilon - \sigma\Delta t}{2\varepsilon + \sigma\Delta t} E^n_{x-\frac{1}{2},i,j,k} + \frac{2\Delta t}{(2\varepsilon + \sigma\Delta t)\Delta y}(H^{n+\frac{1}{2}}_{z,i-\frac{1}{2},j+\frac{1}{2},k} - H^{n+\frac{1}{2}}_{z,i-\frac{1}{2},j-\frac{1}{2},k}) - \frac{2\Delta t}{(2\varepsilon + \sigma\Delta t)\Delta z}(H^{n+\frac{1}{2}}_{y,i-\frac{1}{2},j,k+\frac{1}{2}} - H^{n+\frac{1}{2}}_{y,i-\frac{1}{2},j,k-\frac{1}{2}})$$

$$E^{n+1}_{y,i,j-\frac{1}{2},k} = \frac{2\varepsilon - \sigma\Delta t}{2\varepsilon + \sigma\Delta t} E^n_{y,i,j-\frac{1}{2},k} + \frac{2\Delta t}{(2\varepsilon + \sigma\Delta t)\Delta z}(H^{n+\frac{1}{2}}_{x,i,j-\frac{1}{2},k+\frac{1}{2}} - H^{n+\frac{1}{2}}_{x,i,j-\frac{1}{2},k-\frac{1}{2}}) - \frac{2\Delta t}{(2\varepsilon + \sigma\Delta t)\Delta x}(H^{n+\frac{1}{2}}_{z,i+\frac{1}{2},j-\frac{1}{2},k} - H^{n+\frac{1}{2}}_{z,i-\frac{1}{2},j-\frac{1}{2},k})$$

$$E^{n+1}_{z,i,j,k-\frac{1}{2}} = \frac{2\varepsilon - \sigma\Delta t}{2\varepsilon + \sigma\Delta t} E^n_{z,i,j,k-\frac{1}{2}} + \frac{2\Delta t}{(2\varepsilon + \sigma\Delta t)\Delta x}(H^{n+\frac{1}{2}}_{x,i+\frac{1}{2},j,k-\frac{1}{2}} - H^{n+\frac{1}{2}}_{x,i-\frac{1}{2},j,k-\frac{1}{2}}) - \frac{2\Delta t}{(2\varepsilon + \sigma\Delta t)\Delta y}(H^{n+\frac{1}{2}}_{x,i,j+\frac{1}{2},k-\frac{1}{2}} - H^{n+\frac{1}{2}}_{x,i,j-\frac{1}{2},k-\frac{1}{2}})$$

Apart from the above-mentioned method there are several other ones used for PCF modeling: scattered matrix method, transferred matrix method and others. However mostly used are PWE, FD, and multipole methods for modeling properties of PCFs.

1.5. Properties of single mode photonic crystal fibers

1.5.1. Endlessly single mode fibers:-

PCF can be designed so that they are single mode for a large range of visual and near infrared spectrum. Classical step index fibers (SIFs) always have a cut-off frequency above which the fibers starts to be multimode.

To determine the number of guided modes in SIF usually a normalized frequency V is used. V is defined as:

$$V = \frac{2\pi\rho}{\lambda}\sqrt{n_{core}{}^2 - n_{cladding}{}^2} \qquad (1.2)$$

where ρ is the core radius, $n$core and $n$cladding are refractive indexes of the core and the cladding, respectively.

In the case of standard fibers, the cladding index is almost wavelength in-dependent and V increases when wavelength decreases. It results in multimode operation regime for cut-off normalized frequency higher than 2.405.

1.5.2. Large mode area

Conventional fibers have a strong limit on the core size and the numerical aperture (NA) in a single mode regime. For any wavelength and core diameter there is a maximum NA which makes a single mode regime of operation possible. The value of NA is controlled by the difference in refractive index of the core and the cladding. The fabrication of a standard SIF with a large mode area would require refractive index control in chemical vapor deposition CVD with a very high accuracy (10^{-6} and more), which limits the mode field diameter (MFD) in practice. Usually the MFD of conventional SIF, defined as 1/e width in intensity.

In case of PCF MFD can vary in a single mode regime, depending on requirements. Large mode areas can be engineered by increasing the lattice pitch of the photonic cladding, decreasing the air hole diameter or increasing the size of the defect in photonic cladding (removal of more than one of the central air holes).

1.5.3 Dispersion properties:-

Dispersion of the transmitted signal causes distortion for both digital and analog transmission along the optical fiber. The dispersion mechanisms within the fiber causes broadening of the transmitted light pulses as they travel along the channel. The phenomenon is illustrated in fig where it may be observed that each pulse broadens and overlaps with its neighbours, eventually become indistinguishable at the receiver input.

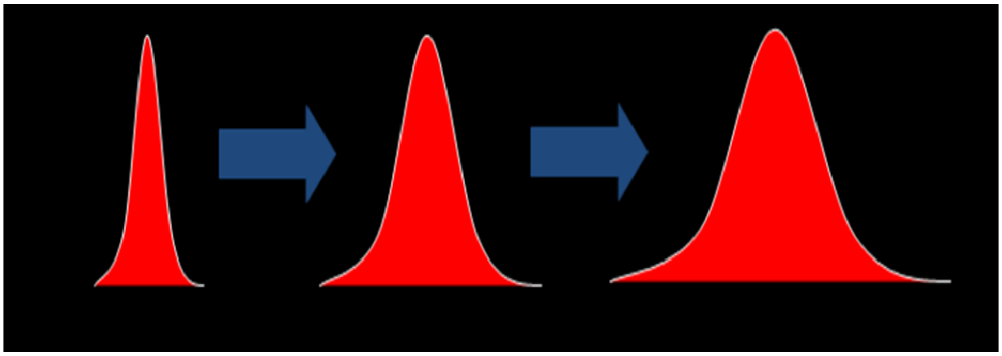

Fig 8 :- Dispersion [4]

In order to appreciate the reasons for the different amounts of pulse broadening within the various types of optical fiber, it is necessary to consider the dispersive mechanism involved. These include material dispersion , waveguide dispersion and intermodal dispersion.

1.5.3.1 Material dispersion:- Pulse broadening due to material dispersion results from the different group velocities of the various spectral components launched into the fiber from the optical source. It occurs when the phase velocity of a plane wave propagating in the dielectric medium varies nonlinearity with wavelength and the material is said to be exhibit material dispersion when the second differential of the refractive index with respect to wavelength is not zero.

.

1.5.3.2 Waveguide dispersion:- The waveguide of the fiber may also create intramodal dispersion. This results, from the variation in group velocity with wavelength for a particular mode. Considering the ray theory approach it is equivalent to the angle between the ray and the fiber axis varying with wavelength which subsequently leads to a variation in the transmission times for the rays, and hence dispersion.

1.5.3.3 Intermodal Dispersion:- Pulse broadening due to intermodal dispersion results from the propagation delay differences between modes within the fiber. As the different modes which constitute a pulse in a multimode fiber travel along the channel at different group velocities, the pulse width at the output is dependent upon the transmission times of the slowest and fastest modes. Thus multimode step-index fibers exhibit a large amount of intramodal dispersion which gives greatest pulse broadening.

1.5.3.4 Group velocity dispersion:-A key parameter that describes properties of fibers is a **group velocity dispersion** (GVD). It is defined as:

$$GVD = \frac{\lambda}{c}\frac{d^2 n_{eff}}{d\lambda^2} \tag{1.3}$$

where n_{eff} is the effective refraction index

$$n_{eff} = \frac{\beta(\lambda, n_m(\lambda))}{k_0} \tag{1.4}$$

Dispersion characteristics in PCFs can be easily shaped due to the flexibility of varying air-hole size and the position in the photonic cladding.

Varying lattice pitch and air-hole sizes in PCFs a zero-dispersion wavelength can be shifted into the visible region.

In case of conventional fibers the zero-dispersion wavelength is limited at a short wavelength side to about 1.3 μm and can be shifted only into longer wavelengths. The fibers with a shifted dispersion are obtained with lower refractive index ring around the core.

If the zero-dispersion wavelength is in the visible region, it automatically gives a positive (anomalous) dispersion in the visible range. PCF with a positive dispersion can be used for dispersion compensation in the telecommunication lines.

At longer wavelength the modal field extends into the holes, thus reducing cladding index as a result PCF can be single moded regardless of wavelength.

1.6 Loss mechanisms:-

The most important factor for any optical fiber technology is loss. The minimum loss in fusedsilica, which is around 1550 nm, is slightly less than 0.2 dB/km. This limit is important, since it sets the amplifier spacing in long-haul communications systems, and thus is a major cost of a long-haul transmission system.

1.6.1 Intrinsic loss:-

The optical loss α(dB), measured in dB/km, of PCFs with a sufficiently reduced con-finement loss, is expressed as:

$$\alpha(\text{dB}) = A/\lambda^4 + B + \alpha_{\text{OH}} + \alpha_{\text{IR}}\,, \qquad (1.5)$$

being A, B, α_{OH}, and α_{IR} the Rayleigh scattering coefficient, the imperfection loss, and OH and infrared absorption losses, respectively. At the present time the losses in PCFs are dominated by *OH*-absorption loss and imperfection loss. In a typical PCF the OH-absorption loss is more than 10 dB/km at 1380 nm and this causes an additional optical loss of 0.1 dB/km in the wavelength range around 1550 nm. Since this contribution is very similar to the intrinsic optical loss of 0.14 dB/km for pure silica glass at this wavelength, the OH-absorption loss reduction becomes an important and challenging problem. Most of the OH impurities seem to penetrate the PCF core region during the fabrication process.

As a consequence, a dehydration process is useful in reducing the OH-absorption loss. Imperfection loss, caused mainly by air-hole surface roughness, is another serious problem. In fact, during the fabrication process, the air-hole surfaces can be affected by small scratches and contamination. If this surface roughness is comparable with the considered wavelength, it can significantly increase the scattering loss. Thus, it is necessary to improve the polishing and etching process, in order to reduce the optical loss caused by this roughness. Moreover, fluctuation in the fiber diameter during the fiber drawing process can cause an additional imperfection loss, if the air-hole size and pitch change along the fiber. It is important to underline that the Rayleigh scattering coefficient of PCFs is the same as that of a conventional SMF. However, this is higher than that of a pure silica-core fiber, although the PCF is made of pure silica glass. It is necessary to reduce the roughness further, in order to obtain a lower imperfection loss and a lower Rayleigh scattering coefficient. It is fundamental to fabricate long PCFs with low loss, if they are to be used as transmission media.

1.6.2 Confinement loss:-

There is also the confinement loss, which is related to the imaginary effective index and decreases very fast with each additional layer of air holes.

$$confinement\ loss[dB/m] = \frac{20X10^6}{\ln 10}\frac{2\pi}{\lambda[\mu m]}\mathrm{Im}\{n_{eff}\} \quad (1.6)$$

be used as transmission media.

1.6.4 Attenuation:-

Attenuation in an optical fiber is caused by absorption, scattering, and bending losses. **Attenuation** is the loss of optical power as light travels along the fiber. Signal attenuation is defined as the ratio of optical input power (P_i) to the optical output power (P_o). Optical input power is the power injected into the fiber from an optical source. Optical output power is the power received at the fiber end or optical detector. The following equation defines signal attenuation as a unit of length:

$$attenuation = (\frac{10}{L})\log_{10}(\frac{P_i}{P_0}) \quad (1.7)$$

Signal attenuation is a log relationship. Length (L) is expressed in kilometers. Therefore, the unit of attenuation is decibels/kilometer (dB/km). As previously stated, attenuation is caused by absorption, scattering, and bending losses.

1.7.Advantages over conventional optical fiber:

1. One interesting feature of PCFs is that many physical properties can be engineered from the microstructure. For example, the waveguide dispersion can be engineered to have the zero dispersion wavelength at any wanted wavelength. This can become extremely interesting for nonlinear applications, where normal dispersion is a limiting factor. By changing the core diameter of suspended-core fibers, the Zero Dispersion Wavelength can be shifted to the visible range. And also, PCFs can be filled with gas or liquids to make optical gas sensors.

2. The nonlinearity of a fiber can be tailored. The effective nonlinearity of a fiber is a function of the nonlinear refractive index as well as the effective area. Since the minimum achievable radius is a function of the numerical aperture, extremely small effective areas are achievable in solid-core fibers, which give huge nonlinearities. In complete contrast, low levels of nonlinearity in hollow-core fibers make them very attractive for high power delivery applications.

CHAPTER 2

NONLINEAR PROPAGATION IN OPTICAL FIBER

2. NONLINEAR PROPAGATION IN OPTICAL FIBER

The nonlinear Schrodinger equation is derived in the followings starting from the Maxwell's equation. The used approximations are discussed in detail and higher order approximations and additional effects are described too. We note that c is used instead of c_0 in further sections because the necessary physical constant we need is the speed of light in vacuum.

2.1 MAXWELL'S EQUATIONS AND WAVE EQUATION:

The complete equation system that can describe all electromagnetic phenomena are the Maxwell's equations whose differential and integral forms are presented Here

$$\nabla \mathrm{x} H = J + \frac{\partial D}{\partial t} \qquad \oint_c H\,dr = \int_s (J + \frac{\partial D}{\partial t})\,ds$$

$$\nabla \mathrm{x}\, E = -\frac{\partial B}{\partial t} \qquad \oint_c E\,dr = -\frac{\partial}{\partial t}\int_s B\,ds \qquad (2.1)$$

$$\nabla B = 0 \qquad \oint_s B\,ds = 0$$

$$\nabla D = \rho \qquad \oint_s D\,ds = \int_v \rho\,dV$$

where H is the magnetic field vector, E is the electric field vector, B and D are the magnetic and electric flux densities, respectively. The current density vector is J and the charge density is ρ. The notation (c) under the sign of the integral means that the integral is carried out for a closed curve, S is for surface and V is for volume.

The corresponding constitutive relations are given by

$$\begin{aligned} D &= \varepsilon_0 E + P \\ B &= \mu_0 H + M \\ J &= \sigma E \end{aligned} \qquad (2.2)$$

where $\varepsilon_0 = 8.885 \times 10{-}12$ As/Vm is the vacuum permittivity, $\mu_0 = 1.2566 \times 10^{-6}$ Vs/Am is the vacuum permeability, σ is the conductibility, its unit of measure is A/Vm, and P and M are the induced electric and magnetic polarizations. In optical fibers the following quantities are zeros: J, ρ (no free charges) and M (nonmagnetic medium). Therefore if we take the curl of Eq. (2.1b) and using eq(2.1a,2.1c,2.1d), yields Eq. (2.3) where we also used the relation $\mu_0\varepsilon_0 = 1/c^2$

$$\nabla X \nabla XE + \frac{1}{c^2}\frac{\partial^2 E}{\partial t^2} = -\mu_0 \frac{\partial^2 P}{\partial t^2} \tag{2.3}$$

There is a well-known vector-analytical relation $\nabla \; X \; \nabla \; X \; E$ for that we can apply in Eq. (2.3):

$$\nabla X \nabla XE \; = \; \nabla (\nabla E) - \nabla^2 E \; = \; -\nabla^2 E \tag{2.4}$$

because the fiber can be considered isotropic and ρ = 0, therefore∇E vanishes (∇D = ε_0∇E= 0). With this substitution Eq. (2.3) becomes:

$$\nabla^2 E - \frac{1}{c^2}\frac{\partial^2 E}{\partial t^2} = \mu_0 \frac{\partial^2 P}{\partial t^2} \tag{2.5}$$

2.2 INDUCED POLARIZATION VECTOR AND SUSCEPTIBILITY TENSOR

In order to solve Eq. (2.5) one has to determine the relation between the induced polarization vector P and electric field vector E. In general, a quantum mechanical approach is needed but if the applied optical frequency is far from the medium resonances which means the wavelength of the field is between 0.5 and 2.2 μm (f_c = 140 − 600 THz) then the electric-dipole approximation is valid. Assuming that the medium response is local, the induced polarization vector can be written as:-

$$P(r,t) = \varepsilon_0 \int_{-\infty}^{\infty} \chi^{(1)}(t-\tau)E(r,\tau)d\tau +$$

$$\varepsilon_0 \int_{-\infty}^{\infty} \int_{-\infty}^{\infty} \chi^{(2)}(t-\tau, t-\theta)E(r,\tau)E(r,\theta)d\tau d\theta + \qquad (2.6)$$

$$\varepsilon_0 \int_{-\infty}^{\infty} \int_{-\infty}^{\infty} \int_{-\infty}^{\infty} \chi^{(3)}(t-\tau,t-\theta,t-\eta)E(r,\tau)E(r,\theta)E(r,\eta)d\tau d\theta d\eta + ...$$

If the medium response is instantaneous compared to the pulse duration ($\tau/T_0 <<$ 1 where T_0 is the pulse width and τ is the nonlinear response time of the medium) then Eq.(2.6) may be approximated by

$$P(r,t) \approx \varepsilon_0[\chi^{(1)}E(r,t) + \chi^{(2)}E(r,t)E(r,t) + \chi^{(3)}E(r,t)E(r,t)E(r,t)] \qquad (2.7)$$

where $\chi^{(j)}$ is the j^{th} order susceptibility, a tensor of rank j + 1.

$\chi^{(1)}$ – is the linear susceptibility. Its effects are included in the linear refractive index n_0 and the attenuation coefficient α.

$\chi^{(2)}$ – is the second order susceptibility. The second order susceptibility is responsible for the second-harmonic generation and sum-frequency generation. It is nonzero only for media that has a lack of inversion symmetry at molecular level. SiO2 is a symmetric molecule, therefore $\chi^{(2)}$ vanishes for silica glasses.

$\chi^{(3)}$ – is the third order susceptibility. It is responsible for the third-harmonic generation, four-wave mixing and nonlinear refraction.

The following notation will be used:

$$P_L = \varepsilon_0 \chi^{(1)} E$$

$$P_{NL} = \varepsilon_0 \chi^{(3)} EEE \tag{2.8}$$

Where:

$$P = P_L + P_{NL} \tag{2.9}$$

and P_L denotes the linear part while P_{NL} the nonlinear part of the induced polarization vector.

2.3DERIVING THE NON-LINEAR SCHRODINGER EQUATION-

We can evaluate now a basic propagation equation from Eq. (2.5) using the (2.8) relations between E and P. Here, we can make some simplifying assumptions:

• P_{NL} is treated as a small perturbation compared to P_L (nonlinear effects are weak in silica fibers).

• The optical field is assumed to maintain its polarization along the fiber length.

• The optical field assumed to be quasi-monochromatic ($\Delta\omega/\omega_0 << 1$ where ω_0 is the center frequency and $\Delta\omega$ is the spectral width).

According to the slowly-varying-envelope approximation it is useful to separate the rapidly varying part of the electric field by writing it in the form of

$$E(r,t) = \frac{1}{2}\hat{x}[E(r,t)\exp(-i\omega_0 t) + E^*(r,t)\exp(i\omega_0 t)] \qquad (2.10)$$

where ˆx is the polarization unit vector of the light assumed to be linearly polarized along the x axis, E(r, t) is a slowly-varying function of time (relative to the optical period) and E* means the complex conjugate of E.

Eq. (2.10) is substituted into Eq. (2.8) and a similar form is used in the polarization vector as in Eq. (2.10):

$$P_L(r,t) = \frac{1}{2}\hat{x}[P_L(r,t)\exp(-i\omega_0 t) + P_L^*(r,t)\exp(i\omega_0 t)] \qquad (2.11)$$

$$P_{NL}(r,t) = \frac{1}{2}\hat{x}[P_{NL}(r,t)\exp(-i\omega_0 t) + P_{NL}^*(r,t)\exp(i\omega_0 t)]$$

A Fourier-transformation is applied on Eq. (2.5) and Eq. (2.11) are substituted and (2.11) in that where we express $P_L(r, t)$ and $P_{NL}(r, t)$ with their relation to E(r, t). The obtained wave equation will have a form of :-

$$\nabla^2 \tilde{E} + \varepsilon(\omega) k_0{}^2 \tilde{E} = 0 \tag{2.12}$$

where ˜E denotes the Fourier-transform of E(r, t), $k_0 = \omega_0/c$ and

$$\varepsilon_0(\omega) = 1 + \tilde{\chi}^{(1)}_{xx} + \frac{3}{4}\tilde{\chi}^{(3)}_{xxxx} \left|E(r,t)\right|^2 \tag{2.13}$$

Eq. (2.12) is known as Helmholtz equation and can be solved by using the method of separation of variables

$$\tilde{E}(r, \omega - \omega_0) = F(x, y)\tilde{E}(z, \omega - \omega_0)e^{i\beta_0 z} \tag{2.14}$$

where ˜E(z, $\omega - \omega_0$) is a slowly varying function of z and F(x, y) is a function which corresponds to the transverse electric modes in the (x, y) plane if the z-axis is identical to the propagation direction. We note here, that both side of Eq. (2.14) contain the E function but at the left hand side it depends on all spatial coordinates while at the right hand side E is only z dependent. In the following, only E(z, t) will be used in the derivation process therefore the argument of the function will not be noted in all cases.

Writing back Eq. (2.14) into Eq. (2.12) we obtain

$$\frac{1}{F}\left(\frac{\partial^2 F}{\partial x^2} + \frac{\partial^2 F}{\partial y^2}\right) + \varepsilon(\omega) k_0{}^2 = \frac{1}{\tilde{E}e^{i\beta_0 z}} \frac{\partial^2 (\tilde{E}e^{i\beta_0 z})}{\partial z^2} \tag{2.15}$$

The two sides of the equation depend on different variables. Therefore the right hand side and the left hand side must be equal with the same constant. Thus we obtain the following differential equations:

$$\frac{\partial^2 F}{\partial x^2} + \frac{\partial^2 F}{\partial y^2} + [\varepsilon_0 k_0{}^2 - \overline{\beta}^2]F = 0$$
$$\frac{\partial^2 \tilde{E}}{\partial z^2} + 2i\beta_0 \frac{\partial \tilde{E}}{\partial z} + [\overline{\beta}^2 - \beta_0{}^2]\tilde{E} = 0 \qquad (2.16)$$

where β is the wavenumber and it is determined by solving the eigenvalue equation (2.16 a). In Eq. (2.16 b), the second derivative can be neglected because $\tilde{E}(z, \omega)$ is a slowly varying function of z.

The eigenvalue β can be written in the form of

$$\overline{\beta}(\omega) = \beta(\omega) + \Delta\beta \qquad (2.17)$$

where $\Delta\beta$ is a perturbation term and $\beta(\omega)$ is the frequency dependent mode- propagation constant. Thus, from Eq. (2.16b) we obtain

$$\frac{\partial \tilde{E}}{\partial z} - \frac{i}{2}\{[\beta(\omega)^2 + 2\beta(\omega)\Delta\beta]\frac{1}{\beta_0} - \beta_0\}\tilde{E} = 0 \qquad (2.18)$$

It is useful to expand $\beta(\omega)$ in a Taylor-series around the carrier frequency ω_0. Writing back the Taylor expanded form of $\beta(\omega)$ to Eq. (2.18) and neglecting the terms that are higher than second order such as $\beta_1\Delta\beta$ and $\beta_2\Delta\beta$. Thus we may obtain the following equation in the Fourier space from (2.18):

$$\frac{\partial \tilde{E}}{\partial z} - i\beta_1(\omega-\omega_0)\tilde{E} - \frac{i}{2}\beta_2(\omega-\omega_0)^2\tilde{E} - i\beta_0\Delta\beta\tilde{E} = 0 \qquad (2.19)$$

Now, performing the inverse Fourier-transformation on Eq. (2.19) and taking into consideration the following equations:

$$F^{-1}\{(\omega-\omega_0)\tilde{E}(z,(\omega-\omega_0)\} = i\frac{\partial E(z,t)}{\partial t} \tag{2.20}$$

and

$$F^{-1}\{(\omega-\omega_0)^2\tilde{E}(z,(\omega-\omega_0)\} = -\frac{\partial^2 E(z,t)}{\partial t^2} \tag{2.21}$$

F^{-1} means the operation of inverse Fourier-transformation. We obtain the next equation

$$\frac{\partial E}{\partial z} + \beta_1\frac{\partial E}{\partial t} + \frac{i\beta_2}{2}\frac{\partial^2 E}{\partial t^2} - i\Delta\beta E = 0 \tag{2.22}$$

The term with $\Delta\beta$ includes the effect of fiber loss and nonlinearity. It can be evaluated from Eq. (2.16 a) using a first-order perturbation theory:

$$\Delta\beta = -\frac{\alpha}{2} + i\gamma|E|^2 \tag{2.23}$$

where γ is the nonlinear coefficient defined by

$$\gamma = \frac{n_2\omega_0}{cA_{eff}} \tag{2.24}$$

A_{eff} is the effective core area in (2.24) which is inversely proportional to the non-linearity. n_2 is the so-called nonlinear refractive index which perturbs the linear index at higher intensities $n = n_0 + n_2 I$.

The effective core area is given in the form of:-

$$A_{eff} = \frac{[\int_{-\infty}^{\infty}\int |F(x,y)|^2 \, dx\,dy]^2}{\int_{-\infty}^{\infty}\int |F(x,y)|^4 \, dx\,dy} \tag{2.25}$$

where $F(x, y)$ is the transverse mode field distribution that can be obtained from the eigenvalue equation (2.16 a). Substituting Eq. (2.23) into Eq. (2.22) and making a variable transformation with

$$T = t - \frac{z}{v_g} = t - \beta_1 z \tag{2.26}$$

one can obtain the NLS equation (2.17). The variable transformation yields the frame moving with the group velocity of the pulse envelope. This is the reduced time useful for describing pulse propagation in a coordinate system fixed to the pulse.

The obtained differential equation describes the light propagation in a lossy, dispersive and nonlinear fiber can be written as

$$\frac{\partial E(z,T)}{\partial z} = -\frac{\alpha}{2}E - \frac{i\beta_2}{2}\frac{\partial^2 E}{\partial T^2} + i\gamma|E|^2 E \tag{2.27}$$

Which is often referred as NLS equation in the case of a = 0. Attenuation is described by the first term at the right-hand side in Eq. (2.27), GVD corresponds to the second term and nonlinearity, or SPM is the third term with the intensity dependence.

In the followings, we describe more general forms of the NLS equation using higher order approximations and including an inelastic stimulated scattering effect.

Higher order dispersion and nonlinearity

Equation (2.27) does not include inelastic scattering such as Raman or Brillouin scattering which becomes important above a threshold of pulse peak intensities and below a certain time duration of the pulses. Raman effect is usually important below the 1 ps time scale if the Raman threshold is reached which can be approximated as follows:-

$$P^{0}_{cr} \approx 16 \frac{A_{eff}}{L_{eff} g_R} \tag{2.28}$$

where $L_{\text{eff}} = (1 - \exp(-\alpha L))/\alpha$ is the effective fiber length with the pulse attenuation α and fiber length L. A_{eff} is the effective core area in Eq. (2.28) and g_{R} is the Raman gain curve as a function of frequency shift. The maximal value of g_{R} is about 10^{-13} m/W for fused silica which is approximately 13.5 THz shift from the reference frequency.

Below 1 ps the spectral width can be broad enough that Raman gain transfers energy from the low-frequency components to the higher frequency components.

This results in the self-frequency shift of the pulse whose physical origin comes from the delayed nature of Raman response.

In this approximation the nonlinear response of the medium is comparable with the pulse width. Thus Eq. (2.14) should be used in the derivation of generalized nonlinear Schrödinger equation (GNLSE). Assuming the following functional form of the nonlinear susceptibility

$$\chi^{(3)}(t-\tau,t-\theta,t-\eta)=\chi^{(3)}R(t-\tau)\delta(t-\theta)\delta(t-\eta) \tag{2.29}$$

where R(t) is the nonlinear response function normalized the same way as the delta function .

Higher order dispersion terms can be easily added including higher order Taylor coefficients from the expansion of $\beta(\omega)$ during the derivation process of (2.27) at the step Eq. (2.18).

Substituting Eq. (2.29) into Eq. (2.6) and performing a similar derivation process to the case of Eq. (2.27) this yields .

$$\frac{\partial E(z,t)}{\partial z}=-\frac{\alpha}{2}E-\left[\sum_{m=1}^{M}\frac{i^{m-1}}{m!}\beta_m\frac{\partial^m}{\partial t^m}\right]E+i\gamma\left(1+\frac{i}{\omega}\frac{\partial}{\partial t}\right)\left(E(z,t)\int_{-\infty}^{\infty}R(t')\left|E(z,t-t')\right|^2dt'\right) \tag{2.30}$$

The response function $R(t)$ includes the electronic (instantaneous) and vibrational (delayed) Raman response

$$R(t)=(1-f_R)\delta(t)+f_Rh_R(t)$$

where f_R is the fractional contribution of the delayed Raman response to the nonlinear polarization and $h_R(t)$ is the Raman response function.

Eq. (2.30) can be simplified with the assumption $\Delta\tau>>10$ fs to the following expression:-

$$\frac{\partial E(z,T)}{\partial z}=\underbrace{-\frac{\alpha}{2}E}_{\text{Loss}}-\underbrace{\left[\sum_{m=2}^{5}\frac{i^{m-1}}{m!}\beta_m\frac{\partial^m}{\partial T^m}\right]E}_{\text{Dispersion}}+i\gamma\left[\underbrace{|E|^2E}_{\text{SPM}}+\underbrace{\frac{i}{\omega_0}\frac{\partial}{\partial T}\left(|E|^2E\right)}_{\text{Self-steepening}}-\underbrace{T_RE\frac{\partial|E|^2}{\partial T}}_{\text{SRS}}\right]$$

where

$$T_R \approx f_R \int_0^{\infty} t h_R(t)\, dt \tag{2.31}$$

where h_R is the Raman response function can be given by an approximate formula which has a Lorentz shape in the Fourier space

$$h_R = \frac{\tau_1^2 + \tau_2^2}{\tau_1 \tau_2} \sin(\frac{t}{\tau_1}) \exp(\frac{-t}{\tau_2}) \tag{2.32}$$

where τ_1 and τ_2 are adjusting parameters with typical values in silica 12.2 fs and 32 fs, respectively.

Using this form of the Raman response function, the integration of Eq. (2.31) can be performed analytically:

$$T_R \approx f_R \frac{2\tau_1 \tau_2}{\tau_1^2 + \tau_2^2} \tag{2.33}$$

This can be used to approximate Raman scattering effect in the last term of (2.30).

2.4 NUMERICAL METHOD

Split-step Fourier method

The Split-Step Fourier (SSF) Method applies the linear propagation (diffraction) operator and index nonhomogeneity in separate steps. The linear propagation operator (ˆL) is applied in the Fourier space and simply represents the k–sphere appropriate to the polarization, direction of propagation and material symmetry. The index nonhomogeneity is a result of a wave guiding structure or third-order nonlinearity.

The SSF method is commonly used to integrate several types of nonlinear partial differential equations. In simulating NLS systems, SSF is predominantly used, rather than finite difference method (FDM), as SSF is often more efficient.

Considering one of the simplest NLS type system, the equation contains the terms of attenuation, dispersion and nonlinearity (See Eq. (2.27)). In order to solve Eq. (2.27) by the SSF method, we write the differential equation in the following functional form

$$\frac{\partial A(z,t)}{\partial z} = [\hat{L} + \hat{N}]A(z,t) \tag{2.34}$$

where ˆL and ˆN are the linear and nonlinear parts of (2.27), respectively, where

$$\hat{L} = -\frac{\alpha}{2} - \frac{i}{2}\beta_2 \frac{\partial^2}{\partial T^2} \tag{2.35}$$

$$\hat{N} = i\gamma |E|^2 \tag{2.36}$$

Integrating (2.34) along z using a small space interval Δz, the solution can be written in the form of

$$E_m(z+\Delta z,t) = \exp\left[\Delta z(\hat{L}+\hat{N})\right]E(z,T), \tag{2.37}$$

where the effects of the linear operator (2.35) can be easily implemented because the time derivatives become multiplications in the Fourier space by: $(i\omega)^n$ where n is the order of the derivative:-

$$\exp[\Delta z L]E(z,t) = \{F^{-1}\exp(\Delta z L(i\omega)]F\}E(z,t) \qquad (2.38)$$

where F denotes the Fourier transformation, F^{-1} the inverse Fourier transformation and $\hat{}L(i\omega)$ is the Fourier transform of $\hat{}L$ which is obtained from Eq. (2.35).

First Order SSF

The essence of the first order SSF method is that the exponential operator acting on E(z, T) in (2.37) is divided into two parts:-

$$E_m(z+\Delta z,t) \approx \exp\left[\Delta z\hat{L}\right]\exp\left[\Delta z\hat{N}\right]E(z,T) \qquad (2.39)$$

The computation of the propagation of the slowly varying envelope is realized in four steps within a space interval Δz:

• Step 1. Nonlinear step: compute $E1 = e^{\Delta z\, \hat{}N}\, E(z, T)$ (by finite differences)

• Step 2. Forward FT: Perform the forward FFT on E_1: $E_2 = FE_1$

• Step 3. Linear step: compute $E3 = e^{(\Delta z \hat{}L)}\, E_2$.

• Step 4. Backward FT: Perform the backward FFT on E_3: $E(z + \Delta z, t) = F^{-1}E_3$.

The Symmetrized (Second Order) SSF

The main difference between the first order Split-Step and the Symmetrized SSF method is that the effect of nonlinearity is included in the middle of the segment. In this procedure the Eq. (2.37) is replaced by

$$E_m(z+\Delta z,t) \approx \exp\left[\frac{\Delta z}{2}\hat{L}\right]\exp\left[\int_z^{z+\Delta z}\hat{N}(z')dz'\right]\exp\left[\frac{\Delta z}{2}\hat{L}\right]E(z,T) \qquad (2.40)$$

where ˆL and ˆN are the linear and nonlinear operators. The integral in (F) can be approximated by the trapezoidal rule.

$$\int_z^{z+\Delta z}\hat{N}(z')dz' \approx \frac{\Delta z}{2}[\hat{N}(z)+\hat{N}(z+\Delta z)] \qquad (2.41)$$

This method can be realized in seven steps within a spatial step Δz:

• Step 1. FFT: $E_1 = F\,E(z, t)$

• Step 2. Half linear step: $E2 = e^{(\Delta z/2\hat{L})}E_1$.

• Step 3. IFFT : $E_3 = F^{-1}E_2$.

• Step 4. Nonlinear step: $E4 = e^{\Delta z\,\hat{N}}\,E_3$

• Step 5. FFT: $E_5 = FE_4$

• Step 6. Other half linear step: $E_6 = e^{\Delta z/2\hat{L}}E_5$

• Step 7. IFFT : $E7 = F^{-1}E_6$

CHAPTER 3

RAMAN AMPLIFICATION

3.1 INTRODUCTION :-

In optical networks, there are many loss mechanisms, including insertion loss, branching loss, and propagation attenuation in silica fibers. Linear optical amplifiers are useful in restoring the power levels of optical signals in the optical domain. Optical amplification in fiber links has been recognized as having major system implications for very long distance transmission of information(>1000Km) using optical fibers and for local distribution systems involving a large number of subscribers. The conventional way of compensating for optical loss in light –wave communication system has been the rather costly and cumbersome procedure of electronic regeneration at the repeater stations. The regeneration process includes photon –electron conversion, electrical amplification, retiming ,pulse shaping and finally electron-photon conversion. In dense wavelength division multiplexed (DWDM) optical networks, there are many frequency channels in a single optical fiber. The conventional way requires the separation of the signals of all the channels for the regeneration, and then recombining all the channels. This is a very expensive approach, particularly for DWDM networks. Optical amplifiers are capable of amplifying the power levels of all the channels simultaneously in optical domain in a manner that is transparent to the modulation format, provided the gain bandwidth is wide enough. This eliminates the need of costly optical-to-electrical and electrical –to– optical conversion at the repeater stations and provides a simple and economical means of bandwidth upgrade in optical networks.

The Raman effect, discovered in 1928 by Sir Chandrasekhar Venkata Raman, is an inelastic scattering of light that is accompanied by elementary excitations in the medium. The principle of Raman amplification is based on the phenomenon of stimulated Raman scattering (SRS). Raman amplification in optical fibers was first observed and measured by Stolen and Ippen. Their measurement showed a frequency shift of approx.13.2THz in a silica fiber. Although Raman amplifiers were demonstrated using solid state lasers, they have not yet been deployed in real field systems.

With the availability of high power diode-pump lasers, the feasibility of Raman amplifier has increased accordingly. Raman amplifiers provide low noise amplification and offer arbitrary gain band.

3.2 RAMAN AMPLIFICATION:-

Raman scattering is a nonlinear effect [12]. Intuition into nonlinear effects can be gained by considering a simple spring. If a small load is attached to a spring, the extension of the spring is linearly related to the load. However, as the load is increased, the dependence of the extension of the spring on the load becomes nonlinearly related to the applied load. Likewise the response of a dielectric medium, such as an optical fiber, to an intense amount of light is nonlinear, and Raman scattering is the result of such a nonlinear process.

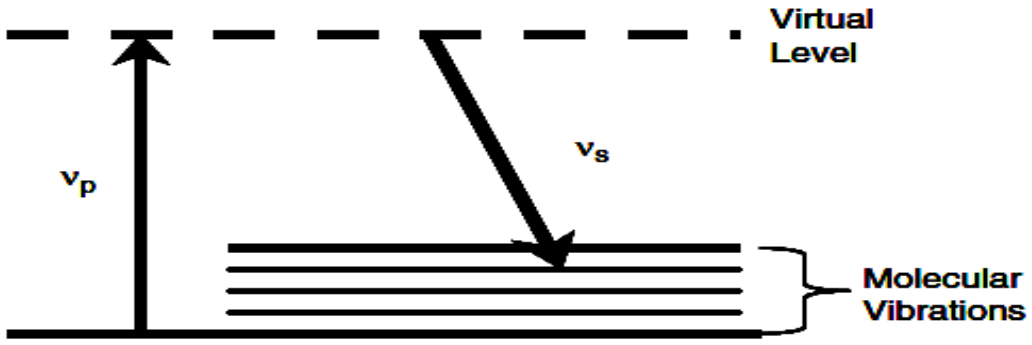

Figure 9**:** Schematic of the quantum mechanical process taking place during Raman scattering. [4]

During Raman scattering, light incident on a medium is converted to a lower frequency [13]. This is shown schematically in Figure 10. A pump photon, v_p, excites a molecule up to a virtual level (non-resonant state). The molecule quickly decays to a lower energy level emitting a signal photon v_S in the process. The difference in energy between the pump and signal photons is dissipated by the molecular vibrations of the host material. These vibrational levels determine the frequency shift and shape of the Raman gain curve. Due to the amorphous nature of silica the Raman gain curve is fairly broad in optical fibers.

For high enough pump powers, the scattered light can grow rapidly with most of the pump energy converted into scattered light. This process is called SRS, and it is the gain mechanism in Raman amplification. Three important points are (i) SRS can occur in any fiber; (ii) because the pump photon is excited to a virtual level, Raman gain can occur at any signal wavelength by proper choice of the pump wavelength; and (iii) the Raman gain process is very fast.

A schematic of an optical telecommunication system employing Raman amplification is shown in Figure 1.2. The signal propagates from the transmitter (Tx) to the receiver (Rx).

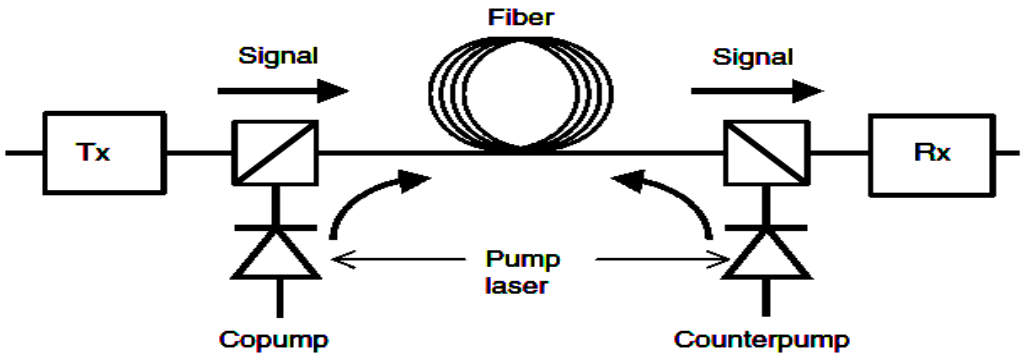

Figure 10: Schematic of an optical communication system employing Raman amplification.[4]

The pump traveling in the same direction as the signal is called the co- or forward pump, and the pump traveling in the opposite direction of the signal is called the counter- or backward pump. When the fiber being pumped is the actual transmission span that links two points, this setup is referred to as a distributed Raman amplifier. If the amplifier is contained in a box at the transmitter or receiver end of the system it is called a discrete Raman amplifier. Another distinctive feature between distributed and discrete Raman amplifiers tends to be the length of the fiber used.

A. Signal-pump Amplification:-

The evolution of the pump, P_p, and signal, P_S , powers along the longitudinal axis of the fiber z in a Raman amplified system can be expressed by the following equations [12]:

$$\frac{dP_s}{dz} = g_R P_p P_s - \alpha_s P_s \tag{3.1}$$

and

$$\pm \frac{dP_p}{dz} = -\frac{\omega_p}{\omega_s} g_R P_s P_p - \alpha_p P_p \tag{3.2}$$

where $g_R(W^{-1}m^{-1})$ is the Raman gain coefficient of the fiber normalized with respect to the effective area of the fiber A_{eff} , $\alpha_{s/p}$ are the attenuation coefficient at the pump and signal wavelength, and $\omega_{s/p}$ are the angular frequencies of the pump and signal. The ± signs represent a co- and counter propagating pump wave, respectively. The first term on the right-hand side of Eq. (3.1) (Eq. (3.2)) represents the signal gain (pump depletion) due to SRS; the second term represents the intrinsic signal (pump) loss. If the depletion of the pump by the signal is ignored, Eq. (3.2) can be solved for the counter propagating case to give ,$P_p(z) = P_0 e^{-\alpha p(L-z)}$, where $P0$ is the input pump power and L is the fiber length. This result is substituted into Eq. (3.2),

$$P_S(L) = P_S(0) \exp(g_R P_0 L_{\text{eff}} - \alpha_S L) \equiv G_N(L) P_S(0) \tag{3.3}$$

where $L_{\text{eff}} = [1 - \exp(-\alpha_p L)]/\alpha_p$, (3.4)

and the resulting differential equation can be solved analytically to yield and G_N is the net gain. Equation (3.3) is a first-order approximation of the signal evolution in the fiber.

The relation between the on–off Raman gain and the Raman gain efficiency is given as :-

$$G_A = \frac{P_s(L)\text{with pump on}}{P_s(L)\text{with pump off}} \tag{3.5}$$

$$= \exp(g_R P_0 L_{\text{eff}})$$

Where P_S *(L)* with pump on is assumed to be the amplified signal power without the amplified spontaneous emission (ASE) and thermal noise with pump on is assumed to be the amplified signal power without the amplified spontaneous emission (ASE) and thermal noise.

B. ASE Noise Figure (NF)

Equation (1) with the pertinent noise term

$$\frac{dP_s}{dz} = -g_R P_p P_s - \alpha_s P_s + 2h\nu\Delta g_R P_p \tag{3.6}$$

The pump power P_p has a simple exponential form in the co Pumping scheme as

$$P_p(z) = P_0 \exp(-\alpha z) \tag{3.7}$$

While in the counter pumping scheme

$$P_p(z) = P_0 ex\,\mathrm{p}\{-\alpha(L-z)\} \tag{3.8}$$

The noise figure can be calculated based on Eqs. (7,8,9) through the following definition:

$$NF(dB) = 10\log(\frac{S_{in}\ /\ N_{in}}{S_{out}\ /\ N_{out}}) \tag{3.9}$$

here *S* and *N* denote the signal and noise parts in optical power at the given frequency, respectively. The optical signal-to-noise ratio (SNR) of the amplified signal is given by:

$$SNR_0 = \frac{P_s(L)}{P_{ASE}} = \frac{G(L)P_{in}}{P_{ASE}} \tag{3.10}$$

$$P_{ASE} = 2\int_{-\infty}^{\infty} S_{ASE}H_f(\nu)d\nu = 2S_{ASE}B_{opt} \tag{3.11}$$

Where B_{opt} is the bandwidth of the optical filter. The factor of 2 in this equation accounts for the two polarization modes of the fiber, and ASE spectral density is defined as:

$$S_{ASE} = n_{SP}h\nu_0 g_R G_L \int_0^L \frac{P_p(z)}{G(z)}$$

CHAPTER 4

SUPERCONTINUUM GENERATION

4.1. INTRODUCTION

The history of photonic crystal fibers (PCFs) started as early as in the seventies . However, its impact remained rather marginal until the nineties when the maturity of the technology enabled the fabrication of almost perfect structures. The great flexibility in the design of PCFs led to tremendous progress in various areas of the field of optics, ranging from frequency metrology to medial science and the future prospects have aroused the interest of many research groups .

Photonic crystal fibers can be classified in two categories: Solid core fiber which guide light as standard optical fibers and Hollow core fibers where the light is confined through the bandgap effect. Solid core fibers could play an important role in optical telecommunications . Indeed, various optical functions ranging from optical switching to wavelength conversion and tunable filters can be performed using Solid core fibers. In particular, the large nonlinearities of these fibers permit these functions to be achieved with a shorter length than when using conventional fibers. Solid core fibers also find applications in laser and amplifier technology . Large core, high numerical aperture and endlessly single-mode Solid core fibers can provide high-power delivery and erbium/ytterbium-doped solid core fibers were recently demonstrated to be efficient for constructing high-power fiber lasers or amplifiers. Poling of Solid core fibers has also been achieved and led to an enhanced second-order susceptibility.

Due to their intrinsic very low nonlinearities and in combination with anomalous dispersion in their transmission band, PBFs allow for high power soliton transmission . Furthermore, the possibility of filling gases into the core of PBFs opens up new prospects for sensor technology , harmonic generation, particle guidance and cold atom guiding.

One of the very first applications of Solid core fibers has been supercontinuum (SC) generation. Supercontinuum is a broadband coherent light source that finds numerous applications in the fields of telecommunication , optical metrology, spectroscopy and medical imaging. In particular, the ultra-broad spectrum of a supercontinuum has allowed for submicron resolution in optical coherence tomography . In metrology, a direct link between the repetition rate of a mode-locked laser and optical frequencies has been established and potential accuracy of 10^{-18} may be achieved in the definition of the second, thus replacing the currently used cesium atom clocks .

In dense-wavelength-division-multiplexing telecommunication systems, a SC can be sliced into hundreds of channels yielding transmission bandwidths of the order of a few terahertz . A supercontinuum can also be utilized for characterization of fiber-optic components or can be used in any application where broadband sources are required.

The first generation of supercontinuum dates back to 1970, when high power picoseconds pulses were focused into a glass sample. Continua were subsequently generated in various gases and liquids. The development of ultra-fast lasers producing trains of short pulses with a wavelength near the minimum dispersion wavelength of optical fibers allowed to generate SC in conventional and specialty fibers. The use of optical fibers for SC generation presents advantages over that of bulk media. In particular, the mode can be confined into a small area, thus enhancing the strength of the nonlinear processes that are responsible for SC formation. Solid core fibers have allowed to go one step further in SC generation.

4.2 SUPERCONTINUUM GENERATION:-

The optical spectrum of a laser pulse train consists of many spectral peaks separated by the repetition rate of the laser. The frequency of the peaks are related to the repetition rate of the pulse train by

$$\omega = \omega_{off} + m.\omega_r \tag{4.1}$$

where ω_r is the repetition rate of the laser, ω_{off} is an offset frequency and m an integer number. In a simple picture, when intense pulses interact with a cubic nonlinear medium, new frequency peaks appear in the optical spectrum of the pulses. The frequencies of these new peaks correspond to the various mixing products of the input frequency peaks

$$\omega_{ijk} = \omega_i + \omega_j - \omega_k \tag{4.2}$$

where ω_{ijk} is the frequency of the new peak and ω_i , ω_j and ω_k correspond to the frequency of the i^{th}, j^{th} and k^{th} peak already present in the spectrum, respectively. Therefore, the cascaded nonlinear processes broaden the optical spectrum of the pump pulses while preserving its comb-like structure. Broad coherent spectra, extending over tens of nanometers and resulting from the broadening of the spectrum of optical pulses in a nonlinear medium, are commonly referred to as supercontinua (SC).

Continua were first generated by focusing high power ps pulses into glass samples . The use of various gases (H2O, D2O, ethylene glycol…) and liquids (water,...) as a nonlinear medium was subsequently demonstrated. The development of tunable mode-locked lasers emitting short pulses led naturally to the use of optical fibers as the nonlinear medium. Indeed, in optical fibers, light can be confined into a very small area, which increases the strength of the nonlinear processes and results in much lower powers needed for SC generation.

4.3 NON LINEAR PARAMETERS INVOLVED IN SUPERCONTINUUM GENERATION:-

SELF PHASE MODULATION :-

Self-phase modulation originates from the intensity-dependence of the refractive index of silica

$$n = n_L + n_2 \left|A\right|^2 \tag{4.3}$$

where n_L is the linear part of the refractive index, $|A|^2$ is the optical intensity and n_2 is the nonlinear- index coefficient related to $\chi^{(3)}$ as

$$n_2 = \frac{3}{8 n_L} \mathrm{Re}(\chi^{(3)}) \tag{4.4}$$

with *Re* standing for the real part and the optical field being assumed to be linearly polarized. A typical value of n_2 for silica material is 3.2×10^{-20} m^2/W. Self-phase modulation refers to the self-induced nonlinear phase shift that an optical pulse experiences as it propagates along the fiber

$$\phi_{NL}^{SPM} = \frac{2\pi L}{\lambda} n_2 |A|^2 \tag{4.5}$$

where L is the length of the fiber. Due to its time-dependence, this nonlinear phase-shift translates into broadening of the optical spectrum as the pulse travels inside the fiber. The temporal shape of the pulse remains unaffected. A useful quantity is the so-called nonlinear length L_{NL} that corresponds to the effective propagation distance at which the maximum phase-shift is equal to 1. It is defined as

$$L_{NL} = \frac{1}{\gamma P_p} \tag{4.6}$$

where P_p is the peak power of the optical pulse and γ the nonlinear coefficient related to n_2 as

$$\gamma = \frac{n_2 \omega_0}{c A_{eff}} \tag{4.7}$$

with A_{eff} being the effective area of the propagating mode inside the fiber and ω the carrier frequency of the optical field. The nonlinear coefficient γ represents the strength of nonlinear effects. Small core solid core fibers exhibit nonlinear effects an order of magnitude higher than conventional fibers.

CROSS-PHASE MODULATION:-

When two optical fields with different wavelengths co-propagate in a nonlinear medium, the refractive index seen by one of the fields not only depends on its own intensity but also on the intensity of the other field. Consequently, the optical field with a center wavelength λ_i experiences a nonlinear phase-shift induced by the co-propagating optical field at wavelength λ_j such that

$$\phi_{NL}^{XPM} = \frac{4\pi L}{\lambda_j} n_2 \left| A_j \right|^2 \tag{4.8}$$

where $|A_j|^2$ represents the intensity of the co-propagating field and L is the interaction length between the two fields. This nonlinear phase-shift is commonly referred to as cross-phase modulation and requires the optical fields to overlap temporally. Equation (43) shows that XPM is twice as effective as SPM.

FOUR WAVE MIXING:-

Four-wave mixing is a nonlinear recombination process of photons of different energies through the third-order susceptibility $\chi^{(3)}$: two pump photons at frequencies ω_1 and ω_2 are annihilated with the simultaneous creation of two new photons at frequencies ω_3 and ω_4.

$$\omega_1 + \omega_2 = \omega_3 + \omega_4 \tag{4.9}$$

The conservation of momentum results in a phase-matching condition to be fulfilled for the process to be efficient

$$\Delta\phi = \left(\frac{n_1\omega_1 + n_2\omega_2 - n_3\omega_3 - n_4\omega_4}{c} + (1 - f_R)\gamma_1(\omega_1)P_{p1} + (1 - f_R)\gamma_2(\omega_2)P_{p2} \right) L = 0 \tag{4.10}$$

where n_j, γ_j, and P_{pj} are the linear refractive index, nonlinear coefficient of silica, and peak power of the optical field at the frequency w_j. Here, L is the fiber length.

A special case referred to as degenerate FWM occurs for $w_1 = w_2 = w_p$. The new generated photons are called Stokes and anti-Stokes photons. This case is of practical interest because when only an intense pump wave propagates along the fiber, Stokes and anti-Stokes waves build up from noise and are subsequently amplified through FWM.

The frequency of the generated Stokes and anti-Stokes waves are such that the energy conservation described by Eq. (4.9) is fulfilled. In terms of propagation constant, the phase-matching condition for degenerate FWM can be expressed as

$$\sum_{k\geq l} \frac{\beta_{2k}}{(2k)!}(\omega_s - \omega_p)^{2k} + (1 - f_R)\gamma(\omega_p)P_p = 0 \qquad (4.11)$$

where w_p and w_s represent the frequency of the pump and Stokes waves, respectively. Here, $\boldsymbol{P}_p$ is the peak power of the pump wave .

STIMULATED RAMAN SCATTERING:-

Stimulated Raman scattering is a photon-phonon interaction. The energy from an intense pump beam is shifted to lower frequencies (Stokes waves) through scattering from vibrational modes of the material molecules. Shifting of energy to higher frequencies (anti-Stokes waves) can also occur but is less efficient

$$2w \longrightarrow w_{as} + w_{st}, \qquad (4.12)$$

with w_p, w_{as} and w_{st} being the frequency of the pump, anti-Stokes, and Stokes photons, respectively.

Stimulated Raman scattering yields gain for a probe wave co-propagating with a pump wave and whose wavelength is located within the Raman gain bandwidth. The normalized Raman gain spectrum of silica is shown in Fig. as a function of frequency difference between the pump and probe waves. The Raman gain of MFs is comparable to that of silica fibers. The gain bandwidth is 40 THz with a peak located at 13.2 THz from the pump frequency.

$$h_R = \frac{\tau_1^2 + \tau_2^2}{\tau_1 \tau_2} \sin\left(\frac{t}{\tau_1}\right) \exp\left(\frac{-t}{\tau_2}\right) \tag{4.13}$$

where τ_1 and τ_2 are the relaxation parameters taken to be 12.2 fs and 32 fs, respectively.

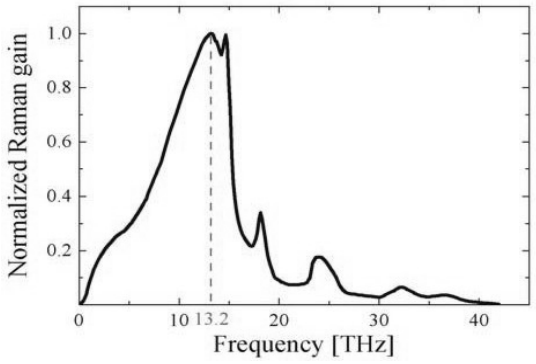

Fig 11:-Normalized Raman gain of silica.**[6]**

SOLITON PROPAGATION ,SOLITON DECAY AND SOLITON SELF FREQUENCY SHIFT

Neglecting the higher-order terms and attenuation, and using convenient transformations, Eq. (32) reduces to

$$i\frac{\partial A}{\partial z} = \frac{1}{2}\mathrm{sgn}(\beta_2)\frac{\partial^2 A}{\partial T^2} - N^2 A|A|^2 \tag{4.14}$$

where *sgn* refers to the sign function and N is defined as

$$N = \sqrt{\frac{L_D}{L_{NL}}} = \sqrt{\frac{\gamma P_p T_0^2}{|\beta_2|}} \tag{4.15}$$

with L_{NL} being the nonlinear length and L_D the dispersion length defined as:-

$$L_D = \frac{T_0^2}{|\beta_2|} \tag{4.16}$$

where T_0 is the temporal width of the pulse related to the full-width at half maximum T_{FWHM} by $T_0=T_{FWHM}$ /1.76. A special case corresponds to negative values of β_2, i.e., when the dispersion is anomalous. In general, Eq. (4.14) can be solved by the inverse scattering method. The solutions define a particular class of waves known as solitons. Among the various types of solitons, a special role is played by solitary waves whose initial symmetric amplitude can be mathematically represented by:-

$$A(T, z=0) = N.\sec h(\frac{T}{T_0}) \tag{4.17}$$

The integer value closest to N is referred to as the soliton order. The case N=1 corresponds to a fundamental soliton, i.e., a state in which the effects of SPM and dispersion are in balance and allows for the wave to maintain its shape as it propagates. The cases $N \geq 2$ corresponds to higher-order solitons. Such waves follow a periodic evolution during propagation with shape recovering at multiples of the soliton period defined as $\pi/2 \cdot L_D$.

Higher-order solitons actually consist of N fundamental solitons, whose relative peak power and temporal width are given by

$$P_k = \frac{(2N-2k+1)^2}{N^2} P_p \qquad T_k = \frac{T_0}{2N-2k+1} \tag{4.18}$$

where k refers to the k^{th} index of the constituent. The fundamental constituents travel together due to the degeneracy of their group-velocities. Higher-order solitons periodically change their shape and spectrum while propagating along the fiber due to interference between the different constituents. Only the degeneracy of the group-velocities binds the constituents of a higher-order soliton together. A small perturbation affecting their relative group-velocities will lead to their subsequent separation. Such process is often referred to as soliton decay or soliton breakup.

These perturbations include higher-order dispersion, the self-steepening effect and stimulated Raman scattering. For a soliton whose temporal width is smaller than 100 fs, the bandwidth of its optical spectrum is 10 THz and, consequently, the spectrum overlaps with the Raman gain. In that case, SRS transfers continuously energy from the blue part of the pulse spectrum to the red part of the pulse spectrum. This energy transfer results in a shift of the center frequency of the soliton towards the infrared as the soliton propagates along the fiber. This process is commonly referred to as the soliton self-frequency shift (SSFS). The magnitude of the Raman-induced SSFS can be approximated by

$$\Delta f = \frac{1.2904\,\lambda_0^{\,2} D(\lambda_0) h(T_0) L}{T_0^{\,4}} \tag{4.19}$$

where T_0 is the temporal width of the soliton and D is the value of the dispersion at the wavelength λ_0. Here, L is the fiber length and $h(T_0)$ represents the overlap integral of the soliton and Raman gain spectra

$$h(T_0) = 496 T_0 \int_0^{\infty} \frac{\Omega^3 R(\Omega / 2\pi T_0)}{\sinh^2(\pi\Omega / 2)} d\Omega \tag{4.20}$$

where $R(\Omega)$ denotes the Raman gain spectrum and Ω the frequency shift from the soliton center frequency. As the soliton propagates along the fiber, its amplitude decreases due to the various loss mechanisms. To counteract this effect, the soliton broadens, which results in slowing-down the frequency-shift rate. Also, variations of dispersion with wavelength and self-steepening contribute to this slowing-down. The soliton eventually reaches a state where its optical spectrum does not overlap with the Raman gain and its center frequency does not shift any further.

SELF –STEEPENING

Self-steepening (SS) results from the dispersion of the third-order susceptibility, i.e., the red frequency components experience a lower nonlinearity than blue frequency components. In the time domain, SS can be thought as the intensity dependence of the group velocity: the peak of the pulse moves at a slower velocity than the wings which induces the trailing edge of the pulse to become steeper as the pulse propagates. In combination with SPM, self-steepening results in a more pronounced broadening of the blue frequency components compared to the red ones. The process of SSFS is substantially reduced by SS since the nonlinearity decreases as the center wavelength of the soliton shifts towards the red.

NONLINEAR PHASE –MATCHED RADIATION:-

The bandwidth of femtosecond solitons exceeds several THz and the variation of dispersion across the soliton bandwidth must be taken into account in the propagation equation:-

$$i\frac{\partial A}{\partial z}+\sum_{k\geq 2}^{\infty}\frac{i^{k}}{k!}\frac{\beta_{k}}{\left|\beta_{2}\right|}\frac{1}{T_{0}{}^{k-2}}\frac{\partial^{k}A}{\partial T^{k}}+N^{2}A\left|A\right|^{2}=0 \qquad (4.21)$$

The terms $k>2$ can be treated as a perturbation for the soliton-like solution of Eq. (4.14). This perturbation makes the solution of Eq. (4.21) very unstable. In particular, linear waves having the same wave-vector as the soliton can co-exist with the soliton. Provided the soliton spectrum overlaps with the frequency of this resonant wave, energy transfer between the linear and solitary waves is possible.

The amplification of the linear wave manifests itself in the optical spectrum as the appearance of a sharp spectral peak in the normal dispersion region of the fiber. The amplitude of the linear wave is proportional to the overlap between the soliton and the linear wave spectra . The frequency of the linear wave ω_R is determined by the phase-matching condition

$$\phi_s - \phi_R = [\beta(\omega_s) - \omega_s\beta_1(\omega_s) + \gamma(\omega_s)P_{ps}]L - [\beta(\omega_R) - \omega_R\beta_1(\omega_s)]L = 0 \qquad (4.22)$$

where f_S and f_r represent the phase of the soliton and resonant wave expressed in a frame moving at the group velocity of the soliton $\beta_1(\omega_s)$. Here, P_{PS} is the peak power of the soliton. Expanding β in Taylor series around ω_s, this phase-matching condition can be rewritten as:-

$$(1 - f_R)\gamma(\omega_s)P_{ps} - \sum_{k\geq 2}\frac{(\omega_R - \omega_s)^k}{k!}\beta_k(\omega_s) = 0 \qquad (4.23)$$

4.4 SUPER CONTINUUM GENERATION IN SOLID CORE FIBERS USING fs PULSES

Supercontinuum is the result of the interplay between the nonlinear effects described in the previous section. Efficient SC generation requires the wavelength of the pump pulses to be in the vicinity of the zero-dispersion wavelength (λ_{ZD}) of the fiber since a high dispersion value tends to limit the magnitude of the nonlinear processes. Small core MFs typically exhibit λ_{ZD} in the range 600-1000 nm. This makes a mode-locked Ti:Sapphire laser a natural candidate for SC generation. Indeed, this type of laser produces intense femtosecond pulse trains at repetition rates varying from tens of MHz to one GHz with a wavelength tunable from 700 to 900 nm. It is also possible to manufacture MFs with λ_{ZD} in the near infrared region and, consequently, SC can be generated using other suitable laser sources such as ytterbium or erbium-doped fiber lasers.

The physics of SC generation in MFs using femtosecond pump pulses strongly depends on the relative detuning between the pump wavelength and the zero-dispersion of the fiber. In particular, different mechanisms are observed depending on whether the pump wavelength is located in the anomalous or normal dispersion region of the fiber.

4.4.1ANOMALOUS PUMPING

To clarify the role played by each nonlinear effect, Eq. (2.30) is solved in the Fourier domain using a standard split-step algorithm with the exact value of the propagation constant. This ensures the validity of the simulation for bandwidth exceeding several hundreds of nanometers.

When only the dispersion is included in the NSE, the pulse corresponds to a higher-order soliton and evolves periodically into a multi-peak structure along the MF. In the presence of higher-order dispersion , the central part of the spectrum initially broadens in the first centimeters of the MF and does not spread any more with further propagation. The most noteworthy feature is the appearance of blue anti-Stokes frequency components in the spectrum. Once they have been generated, these components are not affected by further propagation inside the MF. Adding the Raman term in the equation gives results qualitatively in better agreement with experimental observations, i.e., a strong spreading of the pulse spectrum towards the infrared. The inclusion of the self-steepening term results in an increased magnitude of the anti-Stokes components and reduces the spreading of the spectrum towards the infrared. New anti-Stokes components also appear in the spectrum for longer propagation lengths.

The onset of the supercontinuum formation can be explained as follows: the input pulse corresponding to a *N*th order soliton is compressed in the first few centimeters of the fiber due to SPM. The perturbation of this *N*th order soliton by SRS and higher-order dispersion leads to the breaking up of the *N*th order soliton into multiple fundamental solitons whose amplitudes and widths are given by Eq. (4.18).The red part of the spectra of the multiple solitons overlap with the Raman gain spectrum while their blue part overlaps with the resonant linear waves. As a consequence, the resonant waves are amplified and emerge as anti-Stokes components while the red components get amplified by SRS, which shifts the center frequency of the solitons further to the red. The multiple solitons having different widths, they experience dif-

ferent frequency shifts and appear in the spectrum as distinct Stokes peaks .Since the solitons experience different frequency shifts, they correspondingly experience different group delays and thus appear in the time trace as distinct pulses, the soliton experiencing the largest frequency shift being the originally narrowest soliton and corresponding to the most delayed pulse. The magnitude of the frequency shifts is proportional to the fiber length .

Consequently, the longer the fiber, the more the spectrum spreads towards the infrared . As they propagate along the MF, the various solitons experience losses and dispersion, which results in their temporal broadening. Therefore, their spectrum eventually does not overlap any more with the Raman gain spectrum and the frequency shift ceases. Furthermore, the SS reduces the strength of the nonlinearities as the solitons shifts their center frequency, which results in the decrease of the magnitude of the SSFS with propagation.

4.4.2FACTOR AFFECTING THE BROADENING OF THE SPECTRA:-

EFFECT OF INCREASING THE PUMP POWER:-

An increase of the input pump power results in an enhanced *N*-value. The number of split fundamental solitons therefore increases and more Stokes peaks are observed in the spectrum. Furthermore, the temporal width of the fundamental solitons is reduced (see Eq. (4.18)) and the magnitude of the SSFS is consequently enhanced. The overlap between the solitons and the resonant waves is also larger which results in the increase of the magnitude of the anti-Stokes components. The XPM induced anti-Stokes components shifts also further to the blue since the solitons shifts further to the red. Further increase in the input power eventually leads to a flat spectrum due to the high number of fundamental solitons, with a gap located around λ_{ZD} .

EFFECT OF VARYING PULSE WIDTH:-

Keeping the energy constant while increasing the pulse width results in increasing the number of Stokes peaks and a reduced bandwidth for the generated SC. Indeed, the *N*-value increases proportionally to $\sqrt{T_0}$ leading to the splitting of the input pulse into an increased number of fundamental solitons. These solitons have, nevertheless, broader temporal widths, which results in a decrease of the magnitude of the SSFS. This also means that the overlap between the spectra of the solitons and the resonant wave is reduced and, consequently, the magnitude of the anti-Stokes components is decreased. At high input power values, the SC generated using broader pulses is flatter and exhibit the same bandwidth as the SC generated using narrower pulses due to a higher number of fundamental solitons.

EFFECT OF DETUNING THE PUMP WAVELENGTH:-

When the pump wavelength is tuned closer to λ_{ZD} the *N*-value increases and so does the number of Stokes peaks observed in the spectrum at the output of the MF. The wavelengths of the phase-matched resonant waves lie closer to λ_{ZD} leading to a reduction of the gap observed in the spectrum. The overlap between the solitons and the resonant waves is also increased and, therefore, the magnitude of the anti-Stokes components is enhanced. Initially the solitons lose a lot of energy due to the large overlap with the linear waves, thus resulting in a decrease of the magnitude of the SSFS.

4.5 SUPER CONTINUUM GENERATION IN SOLID CORE FIBERS USING ps AND ns PULSES

Supercontinuum can also be generated in MFs using ps and ns pulses. In this case, the peak power of the pulses is much lower and SPM spectral broadening is negligible. The mechanism leading to SC generation relies on SRS and FWM . Due to the relatively low peak power of the pulses, SC generation requires several meters of MF.

SRS generates a pair of Stokes and anti-Stokes bands in the spectrum which are coupled through parametric FWM. This coupling is much stronger than in conventional fibers due to the high nonlinearity of the MF. This pair can serve as an efficient seed for further parametric amplification, which results in the appearance of multiple side bands in the spectrum. This process is particularly efficient when the pump wavelength is located around λ_{ZD} because the phase-matching condition for
degenerate FWM to occur is then easily fulfilled. The fact that the pulse is ps-broad allows for the pump and side bands to overlap over few meters. Consequently, energy transfers continuously from the pump to the side bands which grow as the pulse propagates along the MF. The different frequency components eventually walk off after few meters of propagation and the spectral broadening ceases. Cross-phase modulation broadens the side bands which subsequently merge, resulting in a smooth spectrum.

Supercontinuum generation using ns pulses has also been demonstrated using frequency-doubled Nd:YAG laser operating at 532 nm or seeded Ytterbium amplifier at 1064 nm. In the case of ns pulses, cascaded Raman scattering is mostly responsible for the generation of the continuum, i.e., multiple lines separated by 13.2 THz are amplified through SRS. For this reason, the spectrum mainly extends towards the infrared. If the pump wavelength is located in the vicinity of λ_{ZD} FWM can contribute to the extension of the SC to the blue wavelengths.

At high enough power all the different Raman lines broaden due to XPM and subsequently merge leading to a smooth spectrum. Since the peak power of ns pulses is typically below the kW level, several meters of MFs are necessary to form the continuum.

CHAPTER 5

SIMULATION RESULTS

Many efforts have been devoted to materials development and design for optical fibers, waveguide devices, fiber lasers and amplifiers to meet the demands of present and future telecommunication systems and other data transmitting services. There is still a strong need and interest to explore fiber materials in order to develop various fiber devices including fiber lasers, amplifiers, optical signal processing devices, etc. Silica fibers are currently used as major waveguide materials in telecom technology. However, they have limited performance if they are applied to active fiber devices. This leads to research focused on new fiber devices using non-silica glasses. Among non-silica glasses, such as heavy metal oxide and non-oxide glasses, tellurite glasses are promising materials for photonics applications, as they combine (i) a wide transmission window, (ii) good glass stability and durability, (iii) high refractive index, (iv) increased nonlinear optical properties, and (v) relatively low phonon energies.

So in this project, i have only focused on research of tellurite fibers. In this project i had done characterization of PCF, Raman amplification and also Supercontinuum generation in Tellurite PCF.

5.1 Characterization Of PCF:-

The refractive index of the tellurite fiber is 2.08. I have design the structure with the help of OPTIFDTD software for the 2μm pitch and D/pitch ratio 0.4 and non linear refractive index for the tellurite fiber is 5.9×10^{-19} m^2W.

With the help of OPTIFDTD software , I have design the structure of PCF for both tellurite and Silica PCF.

Structure parameters:-

Pitch=2µm,

d/Λ=0.4,

n=2.08 for tellurite PCF

n=1.45 for silica PCF

no. of rings=5.

Variation of Effective index, Dispersion and Group index versus wavelength in Telluride glass Photonic crystal Fiber having five rings of air holes.

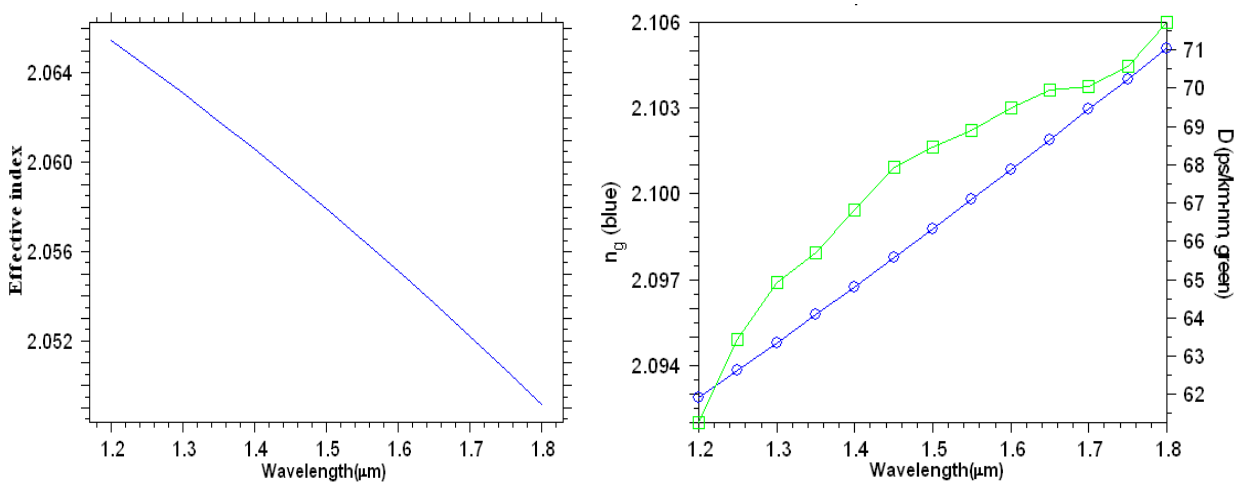

Variation of Effective index, Dispersion and Group index versus wavelength in silica glass Photonic crystal Fiber using same structural parameter as mention above.

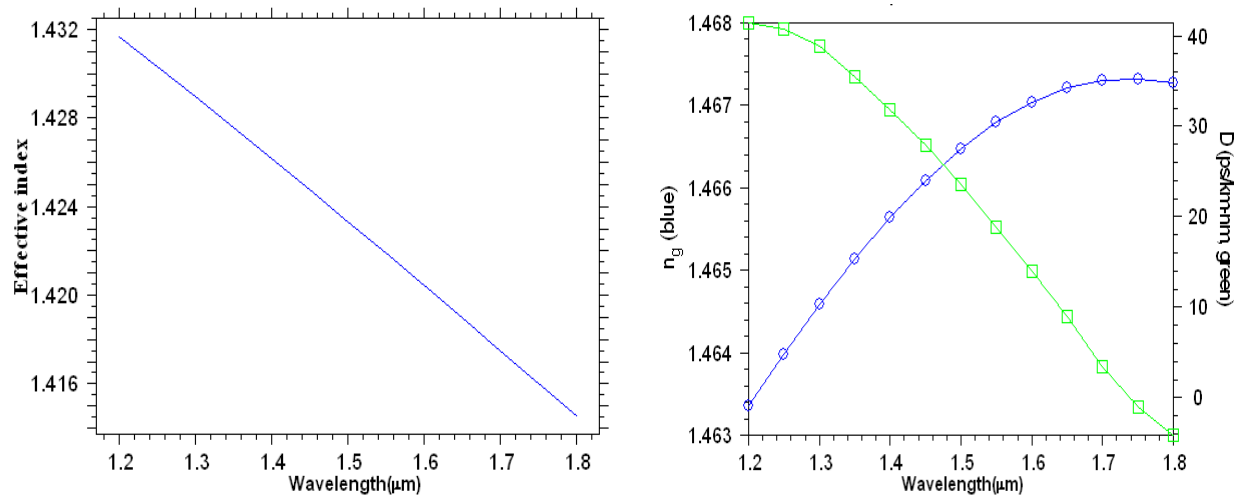

Fig 12:- Variation of Effective index , dispersion and group index with wavelength for tellurite and Silica

Structure use for simulation purpose :-

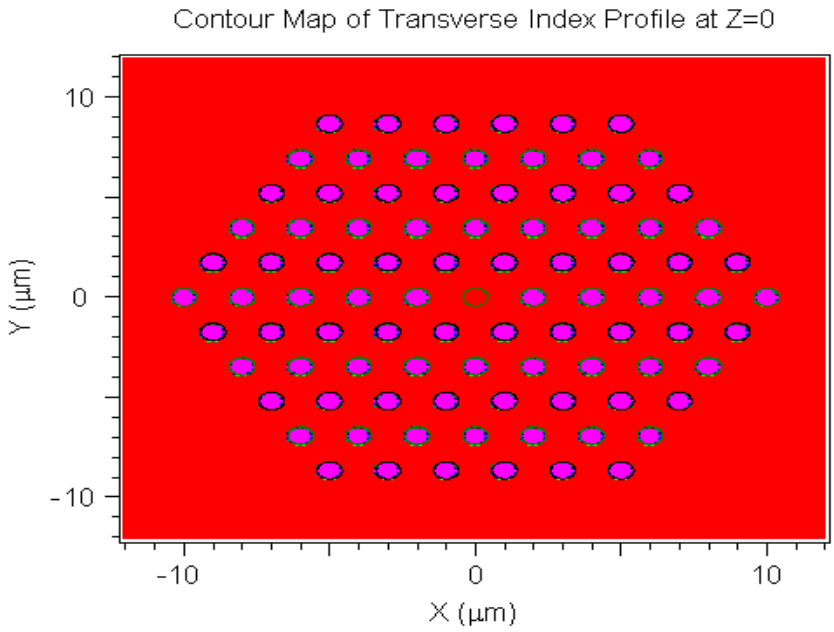

Fig,13:-Structure of PCF used for Stimulation

5.2. Raman amplification :-

In this part I present the Raman amplification characteristics for the tellurite Photonic crystal fiber (PCF) with the RSoft (optisim) Software . In this project I use a small length of the fiber to attain gain characteristics. Numerical simulations reveal that a peak gain of 1.2 dB can be achieved in a 1.1 m long PCF when it is pumped at 1.5 µm in wavelength with an input power of 500 mW. The Raman gain coefficient of tellurite at a 1.5 µm pump wavelength is 6.2×10^{-12} m/W.

Parameters used :-

Signal wavelength :- 1.55µm

Pump wavelength :- 1.50µm

Signal power :- 0.002W

Pump power :- 0.5W

Length of the fiber :- 1.1m

Pitch=2µm,

$d/\Lambda=0.4$,

n=2.08 for tellurite PCF

The following model is used for the stimulation for Raman amplification :-

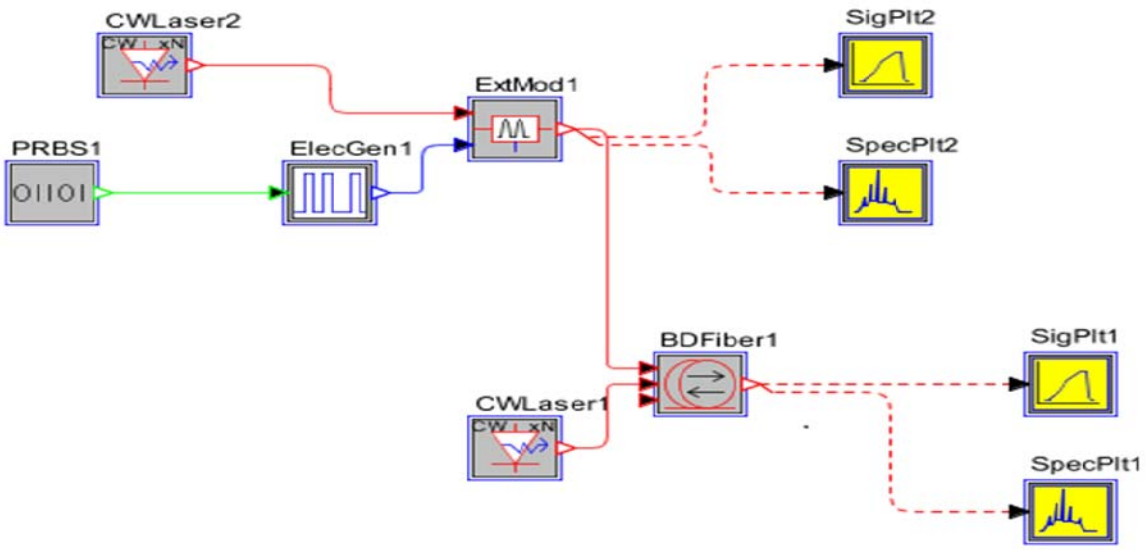

Fig14:- Stimulation diagram for Raman amplification

The gain characteristics for the tellurite fiber and silica fiber are given below :-

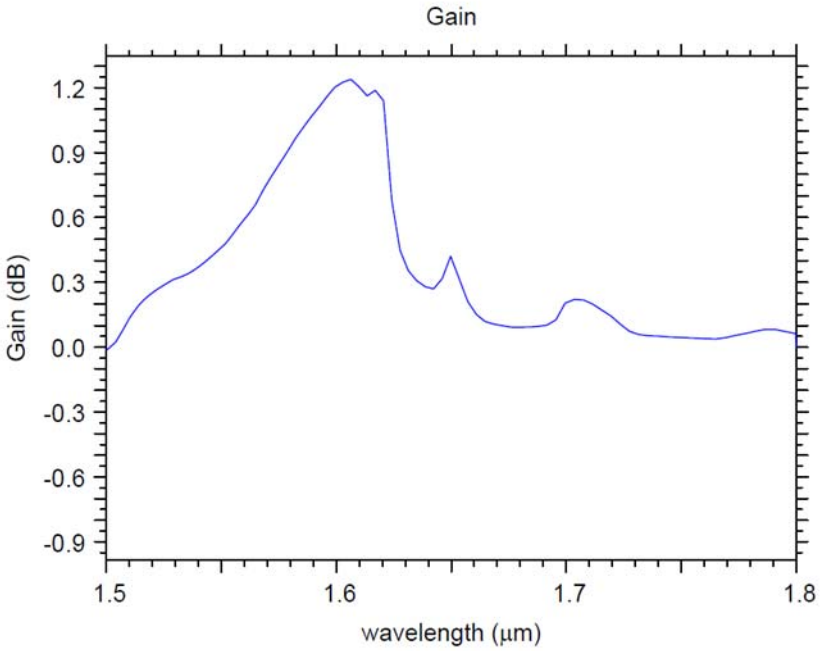

Fig15 :- Gain characteristics for the tellurite fiber

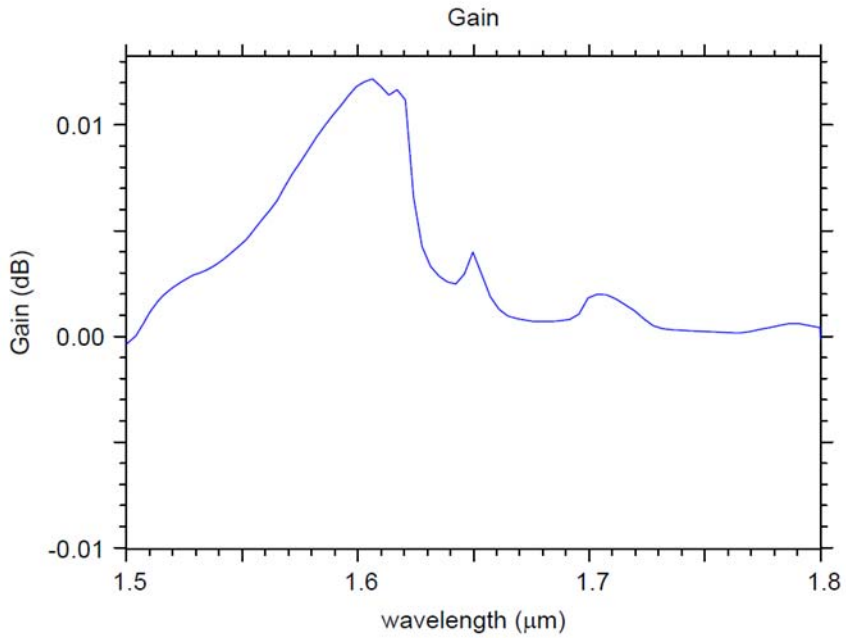

Fig 16 :- Gain characteristics for silica fiber

From the above graph it is clear that the Raman gain in tellurite fiber is higher than the silica fiber which is approximately 10 times .

Now as we increase the length of the fiber the gain increase upto a limit after that the gain become saturated. As shown in the graph the gain become saturated after the 30m length and also we increase the length of the fiber the SNR also decreases.

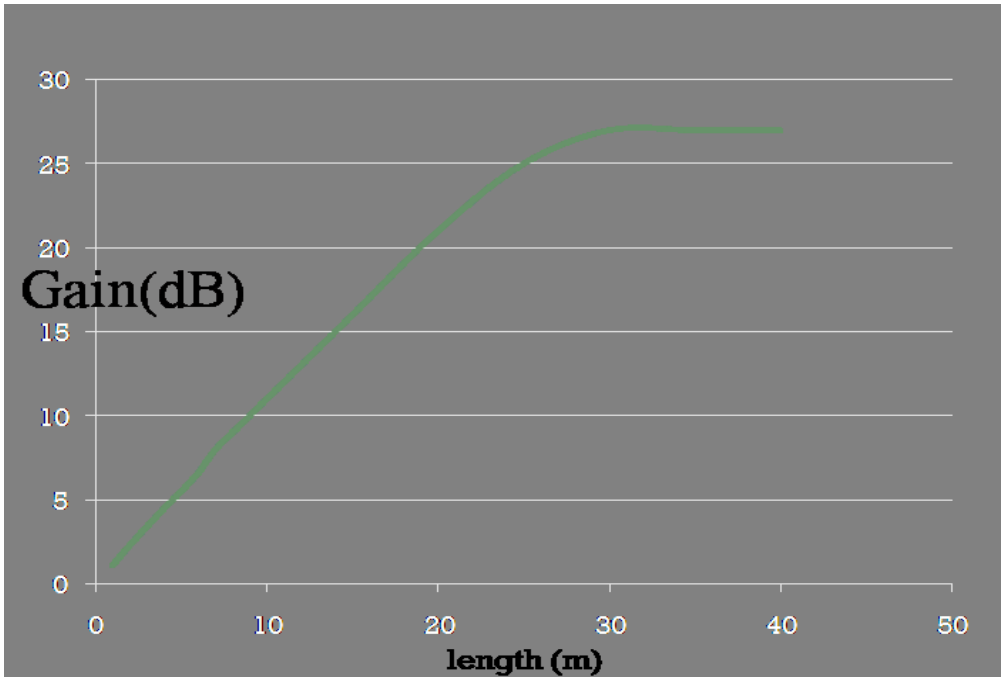

Fig17 :- Gain v/s Length

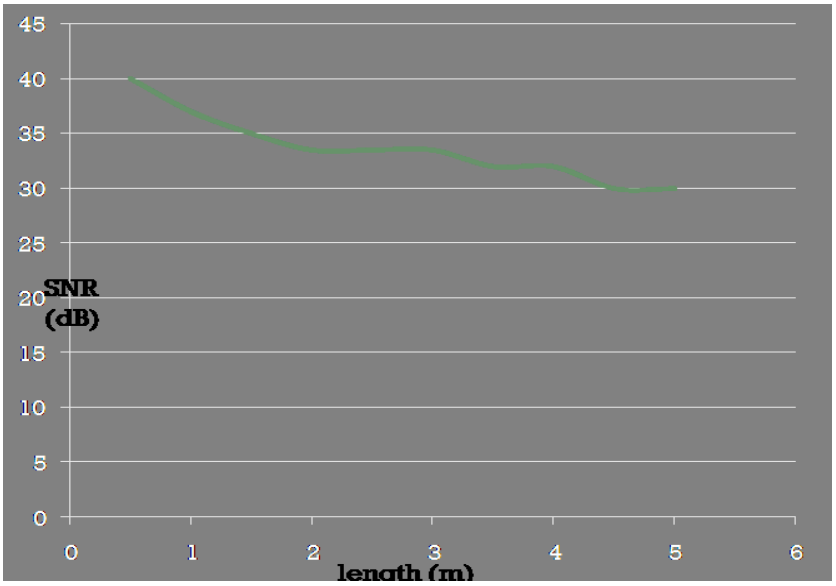

Fig18 :- SNR v/s Length

So I also observe that the as we increase the pitch of the fiber the gain decrease as shown in the graph below:-

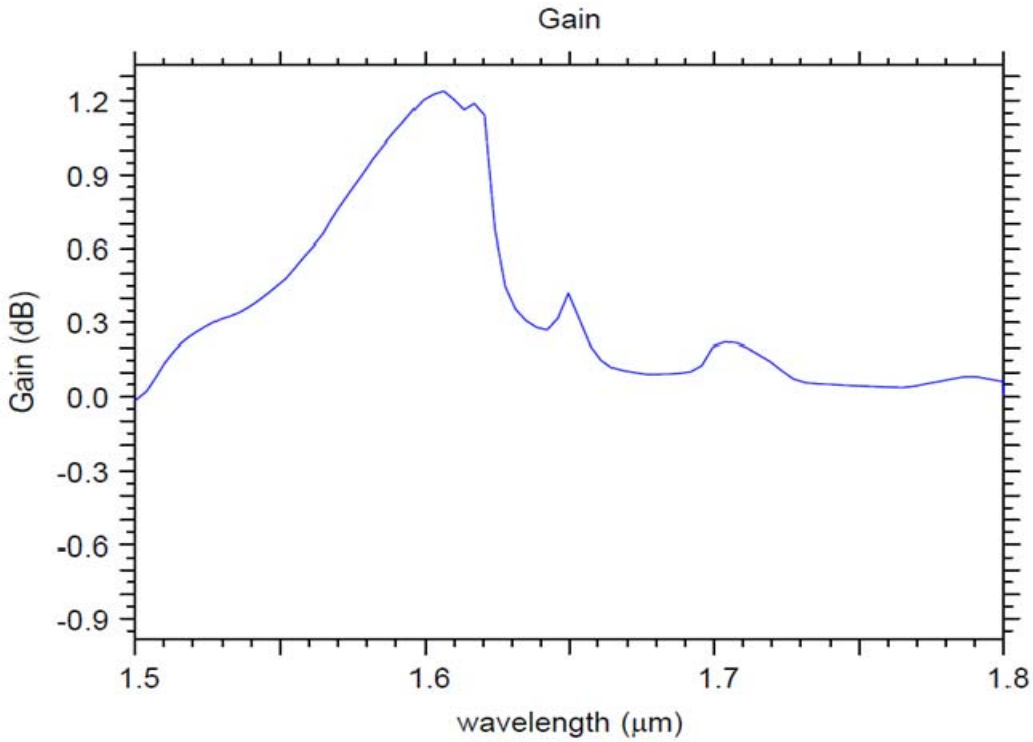

Fig19 :- Gain diagram for Pitch = 2µm

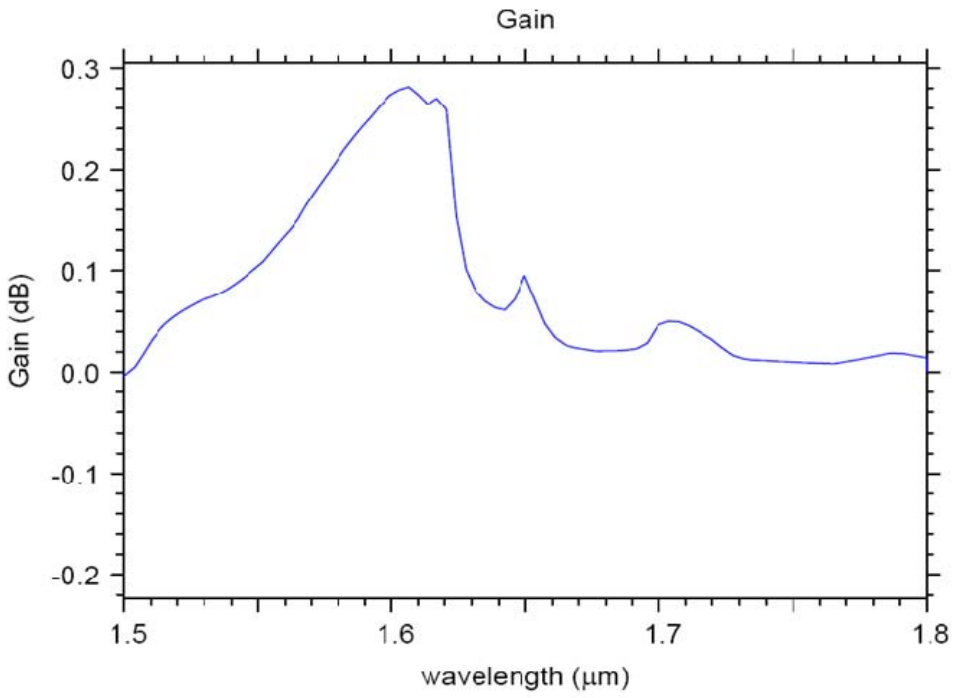

Fig 20 :- Gain diagram for pitch =4μm

5.3. Supercontinuum generation :-

In this part , I present the Supercontinuum generation in the anomalous region.
To simulate Supercontinuum generation RSOFT OPTISIM (software) was used. Optisim software is based on the split step fourier method. And I have also shown the effect of power and FWHM on the broadening . Firstly I compare the result of Dudley et al. (2006), paper with the software . And after getting the match result I have shown the effect of power and FWHM on the broadening.

3.1 Testing the Numerical stimulation program :-

The aim of this project is to generate Supercontinuum generation. Before doing this the program had to be tested against existing experimental and theoretical results in the literature to ensure that the software was producing reliable results.

Comparison of Numerical Simulation with Paper Cases

In this example from Dudley et al. (2006), the Supercontinuum is modeled using the full NLSE , to be compared with the paper results.

Initial Pulse Wavelength=835*nm*

$\gamma=0.11 W^{-1} m^{-1}$

FWHM =50 *fs*

*P*0=10000*W*

$\beta 2=-11.83\ ps^2 m^{-1}$

$\beta 3=8.1038e^{-2}\ ps^3 m^{-1}$

$\beta 4=-9.5205e^{-5}\ ps^4 m^{-1}$

$\beta 5=2.0737e^{-7}\ ps^5 m^{-1}$

$\beta 6=-5.3943e^{-10}\ ps^6 m^{-1}$

$\beta 7=1.3486e^{-12}\ ps^7 m^{-1}$

$\beta 8=-2.5495e^{-15}\ ps^8 m^{-1}$

$\beta 9=3.0524e^{-18}\ ps^9 m^{-1}$

$\beta 10=-1.7140e^{-21}\ ps^{10} m^{-1}$

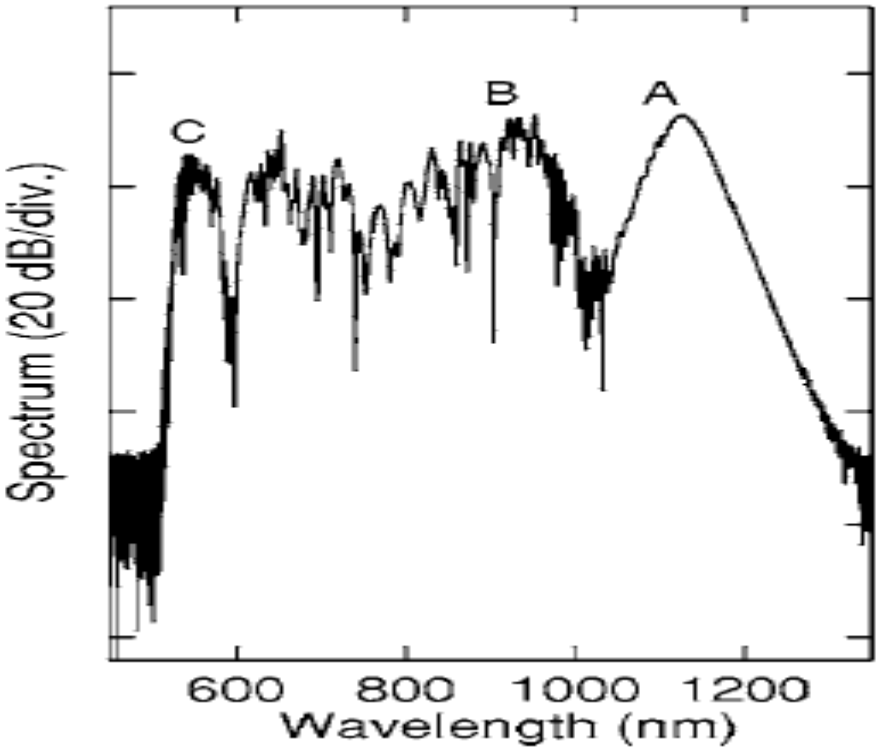

Fig 21:- Spectral plot of an example from Dudley et al. (2006).

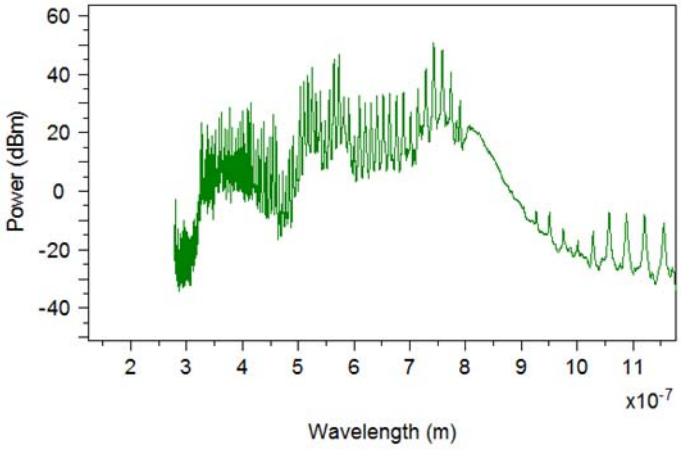

Fig 22:- Simulated spectral plot with the help of optisim software.

Effect of varying the power :- As the pump power increases the broadening of the spectrum increases.

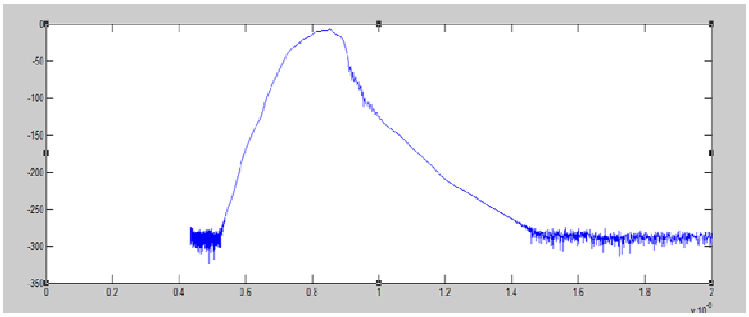

Fig23 (a)

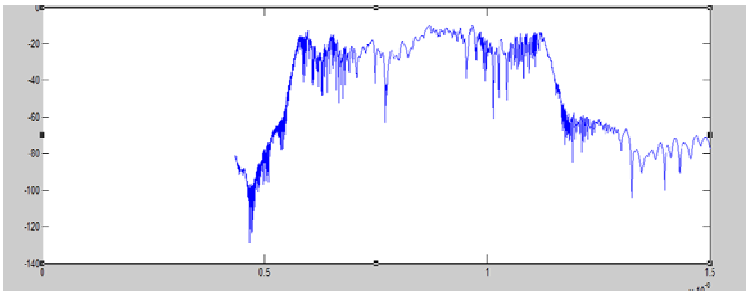

Fig 23 (b)

Fig23 :- effect of power on broadening (a)- 1000W (b) 10000W

Effect of varying pulse width :- By increasing the pulse width the bandwidth of the spectrum decreases.

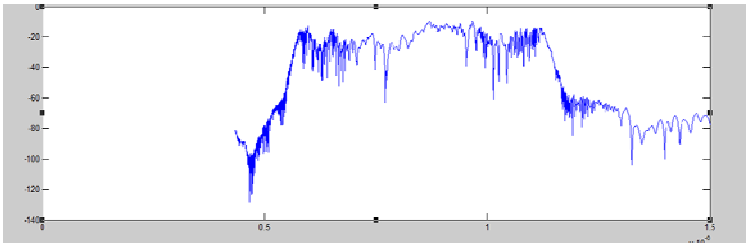

Fig 24(a)

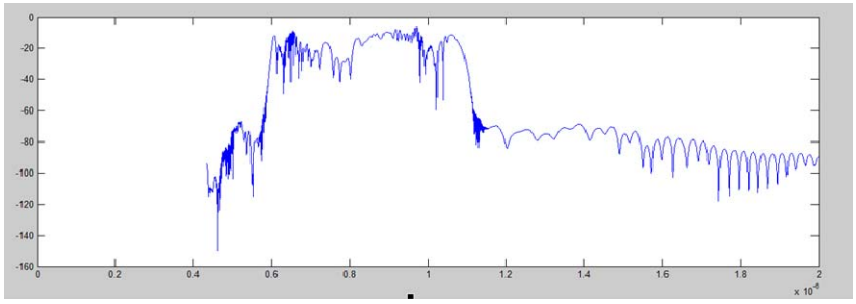

Fig 24 (b)

Fig 24 :- effect of varying pulse width (a)- 100fs (b) - 50fs

6. Conclusion and Future work :-

Conclusion :-

In this thesis, I have used the tellurite fiber whose refractive index and nonlinearity is very high as compared to the silica. In raman amplification the raman gain coefficient is very high as compared to the silica as a result, the gain will be more in tellurite fiber as compared to the silica. Also , the gain attained for a very small length of the fiber. Also shows that how the gain behave with the length and SNR with the length. So as we increases the pitch of the fiber the gain decreases.

For Supercontinuum Generation, in this thesis Supercontinuum is generate in the anomalous region in which the pump wavelength is greater than the Zero dispersion wavelength. I have also shown the effect of varying the power and pulse width on the broadening. As the power increases bandwidth of the spectrum increases and when the pulse width increases the bandwidth of the spectrum decreases.

Future work :-

The next step in this line of research would be mainly experimental. The results from the simulations need to be verified. For the raman gain , verify the result with the matlab programming and also experimentally and also change the material of the fiber like Chalcogenide fiber whose non linearity is very high . For Supercontinuum generation , it can also be verify with the different PCF fiber and also generate the Supercontinuum in normal region and verify the behavior of the Supercontinuum generation with the change of the parameter like power , FWHM and non linear coefficeint with the help of matlab programming.

References :-

1 Dudley, J. M. et al. (2006). Supercontinuum generation in photonic crystal fiber, *Reviews of Modern Physics*, **78**, Number 4.

2 G.P. Agarwal, "Non linear fiber optics", Academic Press, Boston, 198.

3 John Dudley and Roy Taylor, "Supercontinuum generation in optical fibers ",Cambridge university press.

4 A. Ghatak and K. Thyagarajan, "Introduction to Fiber Optics", Cambridge Uni versity Press, 1998.

5 Kuhlmey, Microstructured Optical Fibers: where's the edge?. Optics Express, V. 10 No.22 Nov 2002.

6 R.H. Stolen et. al, "Development of the stimulated Raman spectrum in single-mode silica fibers," J. Opt. Soc. Am. B/vol. 1, no. 4, pp-652-657(1984) .

7 Shailendra K. Varshney, Kunimasa Saitoh, Kento Iizawa, Yukihiro Tsuchida, Ma sanori Koshiba and R. K. Sinha,"Raman amplification characteristics of As_2Se_3 photonic crystal fibers",*Opt. Lett.*, vol. 33, pp. 2431–2433,2008.

8 V. P. Yanovsky, and F. W. Wise, "Nonlinear Propagation of High-Power, Sub-100-Fs Pulses near the Zero-Dispersion Wavelength of an Optical-Fiber", *Opt. Lett.* **19**, 1547-1549 (1994).

9 W. J. Wadsworth, A. Ortigosa-Blanch, J. C. Knight, T. A. Birks, T. P. M. Man, and P. S. Russell,“Supercontinuum generation in photonic crystal fibers and optical fiber tapers: a novel light source”, *J.Opt. Soc. Am. B-Opt. Phys.* 19, 2148-2155 (2002).

10 A. V. Husakou, and J. Herrmann, “Supercontinuum generation, four-wave mixing, and fission of higher order solitons in photonic-crystal fibers”, *J. Opt. Soc. Am. B-Opt. Phys.* **19**, 2171-2182 (2002).

11 J. Herrmann, U. Griebner, N. Zhavoronkov, A. Husakou, D. Nickel, J. C. Knight, W. J. Wadsworth, P. S. J.Russell, and G. Korn, “Experimental evi dence for supercontinuum generation by fission of higher-order solitons in photonic fibers”, *Phys. Rev. Lett.* **88**, (2002).

12 Federica Poli ,Annamaria Cucinotta and Stefano Selleri, “Photonic Crystal Fi ber Properties and Applicatio”, Springer Press, 2007.